Czech Technical University in Prague

Faculty of Nuclear Sciences and Physical Engineering

Department of Physics

DIPLOMA THESIS

Investigation of high-p_T hadron production in interactions with nucleon and nucleus targets

Prague, 2012

Author: Bc. Michal Křelina

Supervisor: RNDr. Ján Nemčík, CSc.

České vysoké učení technické v Praze

Fakulta jaderná a fyzikálně inženýrská

Katedra fyziky

DIPLOMOVÁ PRÁCE

Studium produkce hadronů s velkými p_T v interakcích na nukleonových a jaderných terčících

Praha, 2012

Autor: Bc. Michal Křelina

Supervisor: RNDr. Ján Nemčík, CSc.

Prohlášení

Prohlašuji, že jsem svou diplomovou práci vypracoval samostatně a použil jsem pouze podklady (literaturu, projekty, SW atd.) uvedené v přiloženém seznamu.

Nemám závažný důvod proti užití tohoto školního díla ve smyslu § 60 Zákona č.121/2000 Sb., o právu autorském, o právech souvisejících s právem autorským a o změně některých zákonů (autorský zákon).

V Praze dne _____ _____

podpis

Acknowledgement

I would like to thank RNDr. Ján Nemčík, CSc for his leadership during the preparation of this work, valuable guidance, helpful consultations and for his patience. I want to thank Ing. Jan Čepila for large number of consultations, practical advice and tips. I thank very much Ing. Michal Petráň for language corrections.

I would also like to thank my friends from the Experimental nuclear physics group at FNSPE CTU in Prague, and my parents for their support.

vložit originální zadáníííííííííííííííí !!!!!

Abstract

The inclusive invariant high-p_T hadron production cross section for proton-proton pp and proton-nucleus pA collisions is studied in a QCD improved quark-parton model. For pp collisions we analyse two versions of the model when the initial parton transverse momentum is excluded or included (k_T smearing). Invariant cross sections were calculated for a wide range of c.m. energies and compared with experimental data. For pA collisions we include also nuclear broadening due to initial multiple parton scatterings. We found a nice agreement of the model with RHIC data and performed for the first time predictions for nuclear modification factor at LHC energies.

Key words

QCD, high-p_T particle production, parton model, pp collisions, pA collisions, parton transverse momentum, k_T broadening

Abstrakt

V této diplomové práci je studován inkluzivní invariantní účinný průřez pro produkci částic s vysokou příčnou hybností pro proton-protonové pp a proton-jaderné pA srážky. Pro výpočet účinného průřezu pp srážek byly použity dvě verze QCD partonového modelu s a bez započítání počáteční příčné hybnosti partonů. Výsledky byly spočítané pro celou škálu energií a porovnané s experimentálními daty. Pro výpočet proton-jaderných pA srážek byl použit partonový model rozšířený o počáteční vícenásobný rozptyl v jádře. Vypočítané účinné průřezy byly úspěšně porovnané s daty a také byla spočítaná předpověď pro jaderný modifikační faktor pro LHC.

Klíčová slova

QCD, produkce částic s vysokou příčnou hybností, partonový model, pp srážky, pA srážky, příčná hybnost partonů

Contents

List of Figures

List of Tables

Chapter 1

Introduction

The Quantum Chromodynamics (QCD) is a theory describing strong interactions between hadrons for more than forty years. Basic building blocks of QCD are quarks and gluons. The QCD include two fundamental properties - asymptotic freedom and confinement. It was discovered by D. Gross, F. Wilczek and D. Politzer [1,2] that the asymptotic freedom manifests itself as the interaction of colored particles decreases with an increase of the exchanged momentum (hard processes). However in processes involving small momentum exchanges (soft processes) the effective interactions strength increases and perturbative methods do not work. As a manifestation of non-perturbative phenomenon associated with soft QCD is the absence of free color charges: color particles are confined inside colorless hadrons, i.e. mesons or baryons. Up to now the understanding of the soft QCD dynamics is far from complete.

For typical hadron interactions the underlying QCD theory is probed in the non-perturbative regime and hadronic interactions including various phenomena in nuclear physics cannot be directly derived from the first principles of QCD. The parton model is one of the phenomenological models which can describe such processes.

The experimental investigation of high-p_T phenomena began with using the processes with the simplest kinematics to interpret. These processes include at least one electromagnetic vertex, either e^-e^+ annihilation, deep-inelastic scattering of a lepton on a nucleon, or heavy lepton production in hadron collisions. The electromagnetic vertex is crucial because of its point-like nature. The quark-photon vertex allows to determine kinematics on the parton level.

More complex situation arises when determining short-distance interactions between partons in a hadron. The production of hadrons with large transverse momentum in hadron-hadron collisions can provide useful information for this investigation. Inten-

sive study of these interactions showed that the Quantum Chromodynamics successfully describe experimental data.

During the last decade, the effort to study the nuclear effects, nuclear matter and quark-gluon plasma (QGP) in nucleon-nucleus and nucleus-nucleus collisions increased, especially in ultrarelativistic heavy-ion collisions. High-p_T hadrons are excellent probes into the nuclear matter formed in these reactions. The production of high-p_T hadrons in interactions with nuclei can be helpful for studying effects like the Cronin effect, the shadowing or for the investigation of nuclear parton distribution functions (nPDF).

The main goal of this work is to study high-p_T hadron spectra in the proton-proton (pp) and proton-nucleus (pA) collisions. In the next section the nucleon-nucleon (NN) collision formalism will be reviewed in detail. Both models (the collinear QCD-inspired parton model and the QCD-inspired parton model with the initial parton transverse momentum) are used for the description of the hard scattering processes with large transverse momentum hadrons. At the end of this section, results for pp collisions are calculated and its analysis is presented.

In the third chapter there is the introduction to the nucleon-nucleus (NA) formalism and resultant cross sections for the proton-tungsten and deuteron-gold collisions are presented. Finally, there is presented prediction for nuclear modification factor for LHC's proton-lead collisions. The last section contains the final discussion and summary.

Chapter 2

Nucleon-nucleon collisions

Analyzing high energy nucleon-nucleon NN collisions we adopt the perturbative QCD at the parton level for describing a productions of hadrons with large transverse momenta. Nucleon-nucleon scattering is rather complicated on the level of constituent quarks and gluons, since many subprocesses contribute to the calculation and must be summed over. To calculate the high-p_T hadron production cross section in NN collisions it is necessary to know the momentum distribution of partons inside the hadron i.e. to know the wave function of the parton inside the hadron. Unfortunately, the wave function of the parton inside the hadron cannot be calculated using the perturbative QCD because of its long distance interaction character. But at the same time it is not known how to calculate it even non-perturbatively. It is therefore necessary to use a phenomenological model that connects the calculation of the processes on the parton level using the perturbative QCD and the behavior of partons inside hadrons.

One such model is the parton model. It was formulated by R. P. Feynman [3] and formalized by J. D. Bjorken and E. A. Paschos [4]. The parton model and its application was often reviewed by, for example, R. P. Feynman and G. C. Fox [5], E. Reya [6], J. F. Owens [7] or J. Collins [8]. The parton model originated as a way of understanding deep inelastic scattering (DIS) processes. Further development of the parton model from DIS processes led to the factorization theorem of the QCD [9], which allows application of perturbative calculations to processes involving hadrons.

The hadron-hadron hard scattering process description can be factorized by the factorization theorem to an experimentally measured parton distribution functions (PDF), fragmentation functions (FF) and the partonic differential cross section calculated by the perturbative QCD.

2.1 Parton model

The basic idea of the parton model is that hadrons are made from point-like constituents. This idea comes from results of the SLAC electron scattering experiment at Standford [4]. They investigated deep inelastic processes $ep \to eX$, where e is an incoming resp. scattered electron, p is a target proton and X is a set of final hadrons. The DIS process is illustrated in the Fig. 2.1, where q is a momentum transferred $q = k - k'$ by virtual photon, where k resp. k' are incoming and scattered electron four-momenta and P is a four-momentum of the target proton.

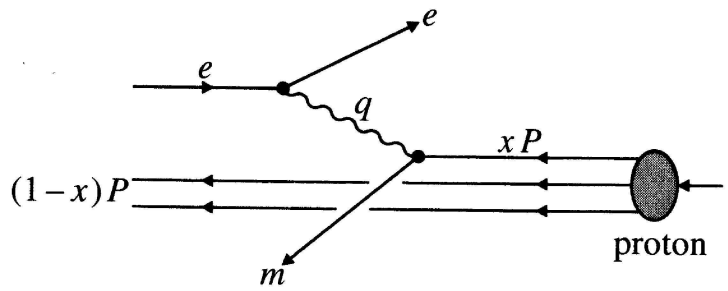

Figure 2.1: Inelastic electron-proton scattering seen in the infinite-momentum frame. Picture is from [10].

Obviously, there are standard variables defined in the DIS

$$\begin{aligned} Q^2 &= -q^2 \\ M^2 &= p^2 \\ \nu &= p \cdot q = M(E' - E) \\ x &= \frac{Q^2}{2\nu} = \frac{Q^2}{2M(E' - E)} \\ y &= \frac{q \cdot p}{k \cdot p} = 1 - E'/E, \end{aligned} \tag{2.1}$$

where E, resp. E' refers to the target rest frame of incoming, resp. outgoing particle, M is the proton mass, Q is momentum transfer, y is the fractional energy transfer from the electron to the proton in the proton's rest frame, x is the Bjorken variable and ν is energy transferred by virtual photon in the proton's rest frame.

Then the electron scattering cross section is [11]

$$\begin{aligned} \frac{d^2\sigma}{dxdy} &= \frac{8\pi\alpha^2 ME}{Q^4} \left[\left(\frac{1 + (1-y)^2}{2} \right) 2xF_1(x, Q^2) \right. \\ &\left. + (1-y)(F_2(x, Q^2) - 2xF_1(x, Q^2)) - (M/2E)xyF_2(x, Q^2) \right], \end{aligned} \tag{2.2}$$

where $F_i(x, Q^2)$ is the structure function which parametrizes the structure of the proton and α is the strong coupling constant.

Experimental results found that the structure functions depend only on x

$$F_i(x, Q^2) \to F_i(x) \tag{2.3}$$

as is illustrated in Fig. 2.2 (for high x). This phenomenon is called the Bjorken scaling. Based on this fact R. P. Feynman interpreted this behavior as a result of the point-like structure of partons. Then, the parton model of DIS was created. This model was formulated in most convenient infinite momentum frame, where the four-momentum of the proton p is $p = (P, 0, 0, P)$ with $P \gg M$. Then the photon scatters off a point-like constituent which is moving collinearly with the proton and which is carrying a fraction ξ of its momentum. Then Eq. 2.2 can be rewritten as

$$\frac{d^2\sigma}{dxdQ^2} = \frac{4\pi\alpha^2}{Q^4}\left[[1+(1-y)^2]F_1 + \frac{1-y}{x}\left(F_2 - 2xF_1\right)\right]. \tag{2.4}$$

By identifying partons as quarks and gluons the $eq \to eq$ elastic scattering can be calculated with final form

$$\frac{d^2\hat{\sigma}}{dxdQ^2} = \frac{4\pi\alpha^2}{Q^4}\left[[1+(1-y)^2]\frac{1}{2}\, e_q^2\delta(x-\xi),\right. \tag{2.5}$$

where e_q^2 is the electron charge. The comparison of Eq. (2.4) and (2.5) yield to a relation for structure functions

$$F_2 = x\, e_q^2\delta(x-\xi) = 2xF_1. \tag{2.6}$$

It means that the structure function $F_2(x)$ describe a quark with the momentum fraction $\xi = x$. This led to the "naive parton model" [3]. Structure functions are obtained by weighting the quark structure functions by the probability distribution $q(\xi)$,

$$F_2 = \sum_{q,\bar{q}} \int_0^1 d\xi\, q(\xi) x\, e_q^2\, \delta(x-\xi) = \sum_{q,\bar{q}} e_q^2\, x\, q(x), \tag{2.7}$$

where $\int_0^1 dx\delta(x-\xi) = 1$.

Final structure function F_2 for the proton for number of flavours $n_f = 4$ can be write as

$$\begin{aligned} F_2(x) &= x\,[(4/9)(u(x) + u_V(x) + \bar{u}(x) + c(x) + \bar{c}(x)) \\ &\quad +(1/9)(d(x) + d_V(x) + \bar{d}(x) + s(x) + \bar{s}(x))\big] \end{aligned} \tag{2.8}$$

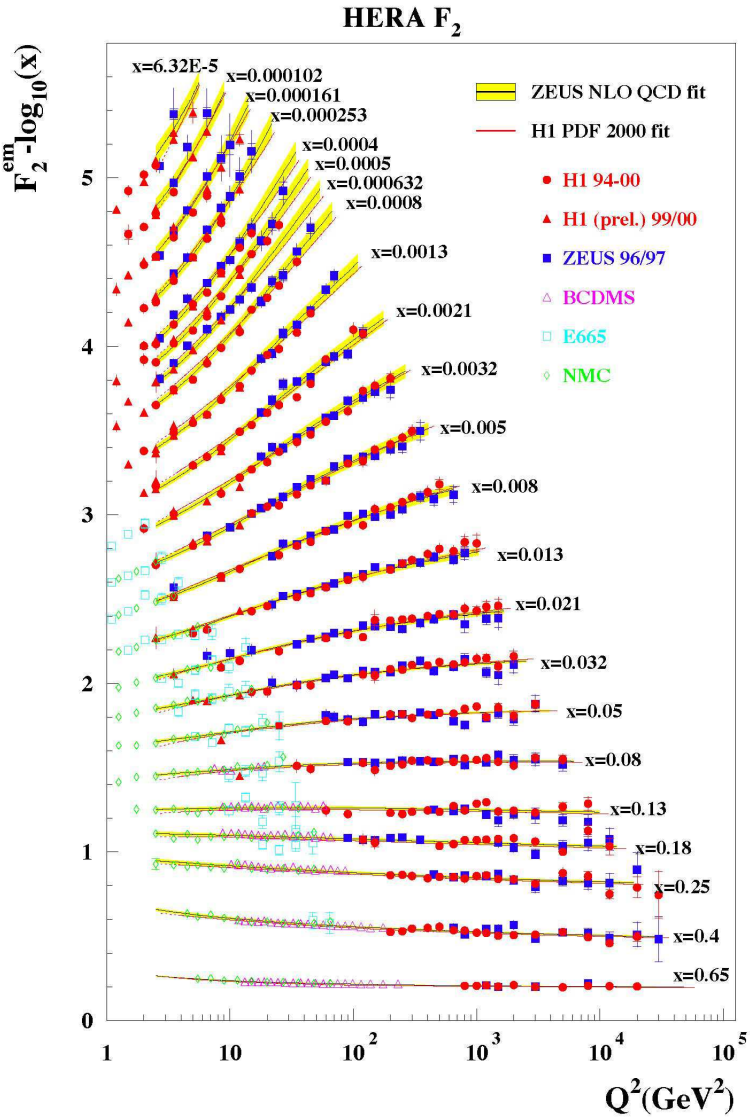

Figure 2.2: The structure function F_2 measured by ZEUS at HERA accelerator. Bjorken scaling violation for low x is presented on this plot.

where $u(x), d(x), s(x), c(x)$ denote quark probability distributions for sea quarks and $u_V(x), d_V(x)$ denote valence quarks of proton (proton contains three valence quarks uud) with sum rules

$$\int_0^1 dx\, u_V(x) = 2 \quad \text{and} \quad \int_0^1 dx\, d_V(x) = 1. \tag{2.9}$$

The valence quarks carry hadrons electric charge and baryon quantum number. Sea quarks are infinite number of virtual $q\bar{q}$ pairs. Fig. 2.3 shows a typical set of quark and

gluon distributions.

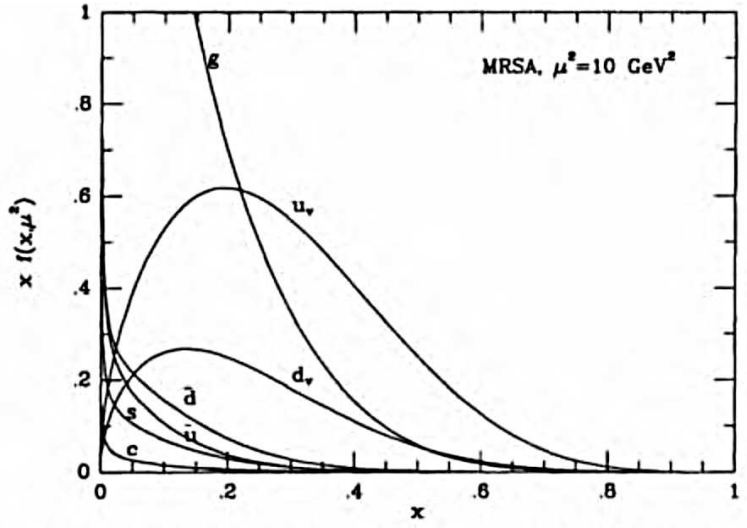

Figure 2.3: Quark and gluon distribution functions at $\mu^2 = 10$ GeV^2, [11].

Further measurements of the DIS at HERA accelerator led to the discovery of the Bjorken scaling violation at low x, showed at Fig. 2.2 (low x). This violation is caused by the fact that quark can emit a gluon. This led to the extension of the parton model to include interactions between the partons via gluon exchange.

This extension of the parton model with a QCD interactions is called a QCD improved quark-parton model. The factorization allows to calculate the cross section as the convolution of perturbative parton cross section and structure functions.

More detailed description of the parton model can be found e.g. in [12].

2.2 Inclusive cross section

A partonic cross section can be approximately described by the leading-order (LO) subprocesses. Leading-order subprocesses correspond to two-body scattering, schematically showed in Fig. 2.4, where A and B denote incoming hadrons, lower-case h_1 and h_2 denote outgoing hadrons and other lower-case letters denote particular partons. The parton distribution function $f_{a/A}(x)$ denotes the probability of finding a parton a in a hadron A with a momentum fraction between x and $x + dx$ and the parton fragmentation function $D_{h/c}$ denotes the probability of obtaining a hadron h with a momentum fraction between z and $z + dz$ from a parton c.

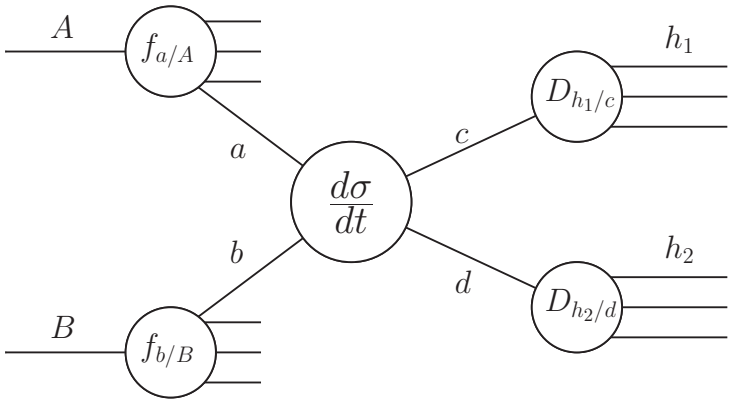

Figure 2.4: Schematic view of the hard scattering process factorized into parton distribution functions (f), parton fragmentation function (D), and the partonic cross section $d\sigma/d\hat{t}$.

The invariant inclusive cross section for the reaction $A + B \to h + X$ for producing a hadron h at high-p_T in the c.m. system of A and B is given by

$$E\frac{d^3\sigma}{d^3p}(AB \to h\,X) = K\sum_{abcd}\int dx_a\,dx_b\,dz_c\,f_{a/A}(x_a,Q^2)\,f_{b/B}(x_b,Q^2)\,D_{h/c}(z_c,\mu_F^2) \times\frac{\hat{s}}{\pi z_c^2}\frac{d\sigma}{d\hat{t}}(ab\to cd)\delta(\hat{s}+\hat{t}+\hat{u}), \quad (2.10)$$

where the sum is over all possible hard subprocesses, K is the normalization factor (more in Sec. 2.4), Q^2 is a square of momentum transfer, μ_F is a fragmentation scale, $d\sigma/d\hat{t}$ is a partonic cross section and the δ function is necessary for the momentum conservation. E, resp. p is energy, resp. momentum of a parton c, $\hat{s}, \hat{t}, \hat{u}$ are parton Mandelstam variables and x_a, x_b, z_c are fraction of momentum of parton inside the hadron (see section 2.5).

2.3 Partonic cross section

The QCD formalism was developed as an extension of the Quantum Electrodynamics (QED) by adding new features e.g. the color charge or the self-interaction of gauge terms. The Lagrangian density has the form

$$\mathcal{L}_{QCD} = \bar{\psi}_i(i\gamma^\mu\partial_\mu - m)\psi_j - gG^a_\mu\bar{\psi}_i\gamma^\mu T^a_{ij}\psi_j - \frac{1}{4}G^a_{\mu\nu}G^{\mu\nu}_a, \quad (2.11)$$

where ψ is Dirac (quark) field, indexes i, j represent the $SU(3)$ gauge group, G^a_μ is a gluon field, g is a coupling constant, γ^μ are Dirac matrices, T^a_{ij} are generators of the $SU(3)$ gauge

group, $G^a_{\mu\nu}$ represent the gluonic field strength tensor $G^a_{\mu\nu} = \partial_\mu G^a_\nu + \partial_\nu G^a_\mu - g f^{abc} G^b_\mu G^c_\nu$, where f^{abc} are the structure constants of $SU(3)$ and m is the mass of quark.

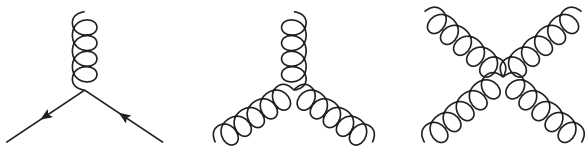

Figure 2.5: Basic vertices of QCD.

The LO means lowest-order calculation of subprocesses at the tree level (order $\mathcal{O}(\alpha_S^2)$) in the perturbative QCD. LO contains just two-body scattering ($2 \to 2$) with two vertices (apart from gluon scattering where graphs with one vertex exists). The Lagrangian density Eq. (2.11) provides three basic vertices showed in the Figure 2.5. All relevant leading-order (LO) diagrams can be created and calculated in perturbative theory from these basic vertices, see Fig. 2.6.

For the calculation of the partonic cross sections at the LO level one has to include 127 independent subprocesses for three quark flavours, for four flavours it is 217 subprocesses and for five flavours it is 331 independent subprocesses. Higher order contributions are discussed in the next section.

The differential cross sections for the hard scattering subprocesses at LO can be written as

$$\frac{d\sigma}{d\hat{t}}\,(ab \to cd) = \frac{\pi \alpha_s^2}{\hat{s}^2} \sum{}^{ab\to cd} \tag{2.12}$$

where $\hat{s}$, $\hat{t}$ and $\hat{u}$ refer to partonic Mandelstam variables and satisfy $\hat{s}+\hat{t}+\hat{u} = 0$, $\sum^{ab\to cd}$ is the cross section with the factor $\pi\alpha_s^2/\hat{s}$ factored out and α_s is the strong running coupling constant. Results for various cross sections appearing in Eq. (2.12) are summarized in Table 2.1.

The running strong coupling constant α_s is dimensionless. It can be written as a function of the square of momentum transfer Q^2 as

$$\alpha_S(Q^2) = \frac{12\pi}{(33 - 2n_f)\ln\left(Q^2/\Lambda^2_{QCD}\right)}\,, \tag{2.13}$$

where n_f is the number of flavours and Λ_{QCD} is a fundamental QCD constant. This coupling constant decreases logarithmically with Q^2 which describes the asymptotic freedom. This means that the coupling constant becomes large at short distance and the perturbative theory can be used.

Subprocess	Cross section
$qq' \to qq'$	$\frac{4}{9}\,\frac{s^2+u^2}{t^2}$
$qq \to qq$	$\left[\frac{4}{9}\left(\frac{s^2+u^2}{t^2} + \frac{s^2+t^2}{u^2}\right) - \frac{8}{27}\,\frac{s^2}{tu}\right]$
$q\bar{q} \to q'\bar{q}'$	$\frac{4}{9}\,\frac{s^2+u^2}{t^2}$
$qq \to qq$	$\left[\frac{4}{9}\left(\frac{s^2+u^2}{t^2} + \frac{u^2+t^2}{s^2}\right) - \frac{8}{27}\,\frac{u^2}{st}\right]$
$gq \to gq$	$\left[-\frac{4}{9}\left(\frac{s}{u} + us\right) + \frac{s^2+u^2}{t^2}\right]$
$q\bar{q} \to gg$	$\left[\frac{32}{27}\left(\frac{t}{u} + ut\right) - \frac{8}{3}\,\frac{t^2+u^2}{s^2}\right]$
$gg \to q\bar{q}$	$\left[\frac{1}{6}\left(\frac{t}{u} + ut\right) - \frac{8}{3}\,\frac{t^2+u^2}{s^2}\right]$
$gg \to gg$	$\frac{9}{2}\left[3 - \frac{tu}{s^2} - \frac{su}{t^2} - \frac{st}{u^2}\right]$

Table 2.1: Table of all LO partonic two-body scattering differential cross sections with factor $\pi\alpha_s^2/\hat{s}$ factored out.

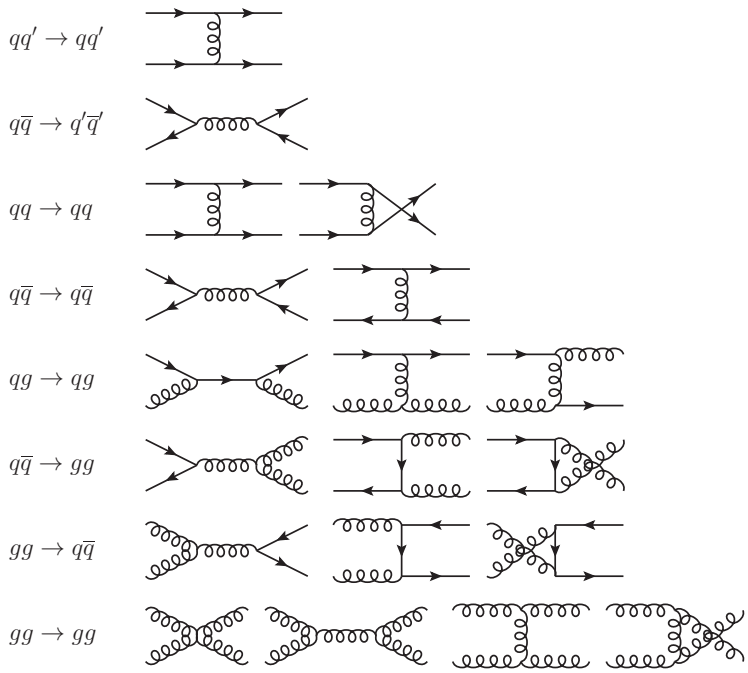

Figure 2.6: The Feynman diagrams for LO partonic subprocesses.

2.4 Higher order calculations and K-factor

Calculations in this work are made at the leading-order only. But data correspond to the sum of all orders of perturbation series. These higher order contributions are relevant for small energies of the collision $\sqrt{s}$ and these higher order contributions decrease with increasing energy $\sqrt{s}$. Generally, adding the higher order contributions means adding

loops and other partons in the final state. Diagrams containing loops (see for example Fig. 2.7), lead to infrared and ultraviolet singularities. It is necessary to eliminate these singularities. That can be done by using regularization and some renormalization scheme. It leads to complex calculations of higher-order terms.

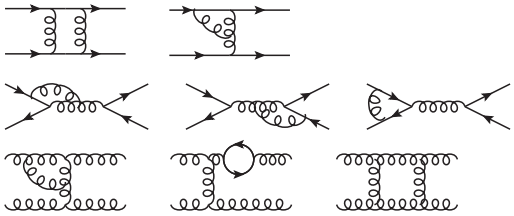

Figure 2.7: Representation of some selected loop graphs.

Next-to-leading order (NLO) calculations include LO processes and ($\mathcal{O}(\alpha_S)$) corrections: $2 \to 3$ body scattering and loop graphs with one loop. For NLO calculations the differential cross section can be written as

$$d\sigma^{NLO} = d\sigma^{LO} + \frac{\alpha_s}{4\pi}\,(d\sigma^{virt} + d\sigma^{real}), \tag{2.14}$$

where $d\sigma^{virt}$ represents one loop virtual corrections and $d\sigma^{real}$ correspond to one gluon or real quark emissions.

To compensate for the differences between the LO and higher order contributions the "K-factor" is established. It can be defined in perturbative series for some processes at the parton level as

$$\sigma_0 + \alpha_S\sigma_1 + ... = K\sigma_0, \tag{2.15}$$

where σ_i are contributions of i-th order, or it can be defined as

$$K = \frac{\sigma^{exp}}{\sigma^{th}}\,, \tag{2.16}$$

where σ^{exp} is the measured cross section and σ^{th} is the calculated cross section.

In the first approximation K can be effectively defined as

$$K = \frac{\frac{d\sigma^{NLO}}{dt}\,(ab \to cd)}{\frac{d\sigma^{LO}}{dt}\,(ab \to cd)} \tag{2.17}$$

for parton level processes. In this paper we consider the K-factor as a function of $\sqrt{s}$. But, Eq. 2.14 implies, that higher corrections are also a function of $\alpha_s(Q^2)$ and therefore a function of the square of the momentum transfer Q^2.

Generally, the K-factor is used to speed up the calculation because including other order adds new terms in thousands. There are several approaches to choose the K-factor.

For example K-factor as an effective function of $\approx \exp(\alpha_s)$ is used in [13]. In [14] K-factor is extracted from jets as a function of $\sqrt{s}$ and $p_{T,jet}$ but in most papers e.g. [15] or [16], it is taken "ad hoc" as a fixed number.

Obviously, the K-factor depends on process in consideration, it varies for pure QCD processes, Drell-Yan processes and for electroweak sector production.

2.5 Kinematics and notation

Note, that for processes $A+B \to C+X$, A and B denote incoming or initial-state hadrons and C denote outgoing or observed final-state hadron. Upper-case letters $(A, B, C, ...)$ describe initial-state and final state hadrons. Their four-momenta p are labeled with corresponding upper-case subscript $(p_A, p_B, p_C, ...)$. Lower-case letters $(a, b, c, ...)$ denote partons and their four-momenta are labeled accordingly $(p_a, p_b, p_c, ...)$.

Longitudinal fractions of hadron momenta carried by respective parton are defined as

$$x_a = \frac{p_a}{p_A}\,, \quad x_b = \frac{p_b}{p_B}\,, \quad z_c = \frac{p_C}{p_c}\,. \tag{2.18}$$

For large transverse momentum processes it is useful to define x-variables

$$x_T = \frac{2p_T}{\sqrt{s}} \quad \text{and} \quad x_F = \frac{2p_l}{\sqrt{s}}\,, \tag{2.19}$$

where p_T is the transverse and p_l is the longitudinal component of momentum with respect to the beam direction. Neglecting the mass of hadrons implies the allowed ranges of x_T and x_l to be $(0, 1)$ and $(0, 1)$ respectively. Next useful variable is the rapidity y, which is defined as

$$y = \frac{1}{2} \ln \frac{E + p_l}{E - p_l}\,. \tag{2.20}$$

For massless particles (mass is negligible for high energy processes), pseudorapidity η is equivalent to the rapidity. Pseudorapidity is defined as $\eta = \ln \cot \theta/2$, where θ is the c.m. scattering angle.

It is beneficial to use Mandelstam variables for hadrons

$$s = (p_A + p_B)^2, \quad t = (p_A - p_C)^2 \quad \text{and} \quad u = (p_B - p_C)^2$$

and for partons

$$\hat{s} = (p_a + p_b)^2, \quad \hat{t} = (p_a - p_c)^2 \quad \text{and} \quad \hat{u} = (p_b - p_c)^2. \tag{2.21}$$

Mandelstam variables satisfy $\hat{s} + \hat{t} + \hat{u} = 0$ for massless partons.

The momentum four-vector of initial-state hadrons is chosen in the simplest form

$$p = (E, \vec{p}) = (E, 0, 0, p_l),$$

where E is the energy of a hadron and p_l is the magnitude of the momentum in the direction of the beam. In the c.m. system it holds $E_A = E_B$ and $p_{l_A} = -p_{l_B}$ for two identical colliding hadrons.

Energy of a colliding hadron can be calculated from the Mandelstam variable

$$s = (p_A + p_B)^2 = 4E^2 \quad \Rightarrow \quad E = \frac{\sqrt{s}}{2},$$

and since for massless particles $E = |\vec{p}|$ holds, so $E = p_l$ and the final form of four-momenta is

$$p_A = \frac{1}{2}\sqrt{s}\,(1, 0, 0, 1) \quad \text{and} \quad p_B = \frac{1}{2}\sqrt{s}\,(1, 0, 0, -1). \tag{2.22}$$

The momentum $\vec{p}_C$ can be separated to the longitudinal and the transverse part $\vec{p}_C = \vec{p}_T + \vec{p}_l$ and so

$$p_C = (E, p_T, 0, p_l) = p_T \left(\frac{E}{p_T}, 1, 0, \frac{p_l}{p_T}\right).$$

The four-momentum can be written as

$$p_C = p_T \left(\frac{E}{\sqrt{E^2 - p_l^2}}, 1, 0, \frac{p_l}{\sqrt{E^2 - p_l^2}}\right) = p_T(\cosh y, 1, 0, \sinh y). \tag{2.23}$$

The proof of last step:

$$\cosh y = \cosh \ln \sqrt{\frac{E + p_l}{E - p_l}} = \frac{1}{2}\left(\sqrt{\frac{E + p_l}{E - p_l}} + \sqrt{\frac{E - p_l}{E + p_l}}\right) = \frac{E}{\sqrt{E^2 - p_l^2}}$$

and

$$\sinh y = \sinh \ln \sqrt{\frac{E + p_l}{E - p_l}} = \frac{1}{2}\left(\sqrt{\frac{E + p_l}{E - p_l}} - \sqrt{\frac{E - p_l}{E + p_l}}\right) = \frac{p_l}{\sqrt{E^2 - p_l^2}}.$$

Next, the application of Eq. (2.18) to the Eq. (2.22) and (2.23) yields to

$$p_a = \frac{1}{2}\,x_a\sqrt{s}(1, 0, 0, 1) \quad p_b = \frac{1}{2}\,x_a\sqrt{s}(1, 0, 0, -1) \quad \text{and} \quad p_c = \frac{p_T}{z_c}\,(\cosh y, 1, 0, \sinh y). \tag{2.24}$$

Now, it is appropriate to express the parton Mandelstam variable as

$$\begin{aligned}
\hat{s} &= (p_a + p_b)^2 \\
&= \left(\frac{\sqrt{s}}{2}\,(x_a + x_b, 0, 0, x_a - x_b)\right)^2 \\
&= \frac{s}{4}\left[(x_a + x_b)^2 - (x_a - x_b)^2\right] \\
&= x_a x_b s,
\end{aligned}$$

$$\begin{aligned}
\hat{t} &= (p_a - p_c)^2 \\
&= \left(\frac{x_a\sqrt{s}}{2} - \frac{p_T}{z_c}\cosh y, -\frac{p_T}{z_c}, 0, \frac{x_a\sqrt{s}}{2} - \frac{p_T}{z_c}\sinh y\right)^2 \\
&= \frac{p_T^2}{z_c^2}\left(\cosh^2 y - \sinh^2 y - 1\right) + \frac{x_a\sqrt{s}}{z_c}\,p_T(\sinh y - \cosh y) \\
&= -\frac{x_a}{z_c}\sqrt{s}p_T e^{-y}
\end{aligned}$$

and evaluation of the $\hat{u}$ is very similar to the $\hat{t}$. Finally, the summary of all Mandelstam variables on the parton level is presented

$$\hat{s} = x_a x_b s, \quad \hat{t} = -\frac{x_a}{z_c}\,p_T\sqrt{s}\,e^{-y} \quad \text{and} \quad \hat{u} = -\frac{x_b}{z_c}\,p_T\sqrt{s}\,e^{y}. \tag{2.25}$$

Next, Eq. (2.25) can be used to evaluate the δ function in the Eq. (2.10)

$$\begin{aligned}
\delta(\hat{s} + \hat{t} + \hat{u}) &= \delta\left(\hat{s} - \frac{x_a}{z_c}\sqrt{s}p_T e^{-y} - \frac{x_b}{z_c}\sqrt{s}p_T e^{y}\right) \\
&= \delta\left[\frac{1}{z_c}\left(z_c\hat{s} - x_a\sqrt{s}p_T e^{-y} - x_b\sqrt{s}p_T e^{y}\right)\right] \\
&= z_c\delta\left[\hat{s}\left(z_c - \frac{p_T}{\sqrt{s}x_b}\,e^{-y} - \frac{p_T}{\sqrt{s}x_a}\,e^{y}\right)\right] \\
&= \frac{z_c}{\hat{s}}\,\delta\left(z_c - \frac{x_T}{2x_b}\,e^{-y} - \frac{x_T}{2x_a}\,e^{y}\right)
\end{aligned}$$

and to integrate Eq. (2.10) over z_c

$$z_c = \frac{x_T}{2x_b}\,e^{-y} + \frac{x_T}{2x_a}\,e^{y}. \tag{2.26}$$

Then, by applying the upper boundary condition $z_c \leq 1$ to (2.48) the minimal value of x_b is obtained

$$x_{b_{min}} = \frac{x_a x_T e^{-y}}{2x_a - x_T e^{y}} \tag{2.27}$$

and similarly by applying of the upper boundary condition $x_b \leq 1$ the minimum of x_a is obtained

$$x_{a_{min}} = \frac{x_T e^y}{2 - x_T e^{-y}}\,. \tag{2.28}$$

If the last condition $x_a \leq 1$ is applied, the general kinematic restriction is obtained

$$\cosh y \leq \frac{\sqrt{s}}{2p_T}\,. \tag{2.29}$$

Finally, by evaluating the δ function in (2.10), integrating over z_c (2.48) and by application of the minimal value of x_a (2.28) and x_b (2.27) the following final expression can be obtained

$$\begin{aligned} E\frac{d^3\sigma}{d^3p}\,(AB \to h\ X) \;&=\; K \sum_{abcd} \int_{x_{a_{min}}}^{1} dx_a \int_{x_{b_{min}}}^{1} dx_b\, f_{a/A}(x_a, Q^2)\, f_{b/B}(x_b, Q^2) \\ &\quad \times D_{h/c}(z_c, \mu_F^2) \frac{1}{\pi z_c} \frac{d\sigma}{d\hat{t}}\,(ab \to cd), \end{aligned} \tag{2.30}$$

where

$$z_c = \frac{x_T}{2x_b}\, e^{-y} + \frac{x_T}{2x_a}\, e^{y}, \quad x_{b_{min}} = \frac{x_a\, x_T\, e^{-y}}{2x_a - x_T\, e^{y}} \quad \text{and} \quad x_{a_{min}} = \frac{x_T\, e^{y}}{2 - x_T\, e^{-y}}\,. \tag{2.31}$$

2.6 Parton distributions and fragmentation functions

The factorization theorem implies the independence of parton fragmentation and distribution functions on the scale Q^2. That allows to obtain both functions by fitting data from the deep-inelastic scattering or $e^- e^+$ annihilation. These fits were obtained at relevant factorization scales Q^2 for parton distribution function, resp. fragmentation scale μ_F for fragmentation function and for other scales it can be calculated by the DGLAP (Dokshitzer-Gribov-Lipatov-Altarelli-Parisi) evolution equations [17–19]

$$\frac{df_{q_i/A}(x, Q^2)}{dt} = \frac{\alpha_s(Q^2)}{2\pi} \int_x^1 \frac{dy}{y} \left[P_{qq}(x/y) f_{q_i/A}(y, Q^2) + P_{qg}(x/y) f_{q_i/A}(y, Q^2)\right] \tag{2.32}$$

and

$$\frac{df_{g/A}(x, Q^2)}{dt} = \frac{\alpha_s(Q^2)}{2\pi} \int_x^1 \frac{dy}{y} \left[\sum_i P_{gq}(x/y) f_{q_i/A}(y, Q^2) + P_{gg}(x/y) f_{g/A}(y, Q^2)\right], \tag{2.33}$$

where $f(x, Q^2)$ is the distribution function of a quark or a gluon, t is defined as $\ln(Q^2/\Lambda^2_{QCD})$ and P_{ij} are splitting functions.

The function $P_{p'p}$ represents the probability that a parton of type p radiates a quark or gluon and becomes a parton of type p' carrying fraction x/y of the momentum of parton.

The general procedure for obtaining the distribution function is as follows. First, xf_i dependence on x at some initial value of Q_0^2 is parameterized and then the evolution equations (2.32) and (2.34) are used. Using minimization procedure free parameters and coupling constant α_s are determined. Usually, xf_i is expressed as

$$xf_i = a_i\, x^{b_i}(1-x)^{c_i}, \tag{2.34}$$

where a_i, b_i and c_i are free parameters.

In this work the following parton distribution functions were used: CTEQ6 (2002) [20], MSTW2008 (2008) [21] and NNPDF2.1 (2011) [22]. The illustrative comparison of these parton distribution functions is showed at the Fig. 2.8.

The CTEQ6 parton distribution function offers LO and NLO for $n_f = 5$ with restrictions $10^{-8} < x < 1$ for the Bjorken x and $1.3 < Q < 10^5$ GeV for the scale. The MSTW2008 parton distribution function offers LO, NLO and NNLO for $n_f = 6$with restrictions $10^{-6} < x < 1$ for the Bjorken x and $1 < Q^2 < 10^9$ GeV^2 for the scale. MSTW2008 also contains distribution for the photon. The NNPDF2.1 PDF parton distribution function offers LO, NLO and NNLO for $n_f = 6$ with restrictions $10^{-9} < x < 1$ for the Bjorken x and $2 < Q^2 < 10^8$ GeV^2 for the scale.

The fragmentation of partons into hadrons can be explained only using models. The most used model is the independent fragmentation model (IFM) [23]. For full description of the final state event generators based on string or cluster models are needed. Data for fragmentation functions were obtained primarily from e^-e^+ collisions at e.g. KEK, DESY, SLAC or CERN.

The following fragmentation functions were used: KKP [24] (Kniehl-Kramer-Pötter, 2000), DSS [25] (de Florian-Daniel-Sassot, 2007) and Kretzer [5] (2000). Comparison of fragmentation functions is shown in Figure 2.9.

KKP provides fragmentation into pions, kaons, nucleons, anti-nucleons and charged hadrons in LO and NLO for $n_f = 5$ with restrictions $0.1 < x < 0.8$ (otherwise interpolated) for the Bjorken x and $2 < Q^2 < 10^4$ GeV^2 for the scale. DSS provides fragmentation into pions, kaons, protons, anti-protons and charged hadrons in LO and NLO for $n_f = 5$ with restrictions $0.05 < x < 1$ for the Bjorken x and $1 < Q^2 < 10^5$ GeV^2 for the scale.

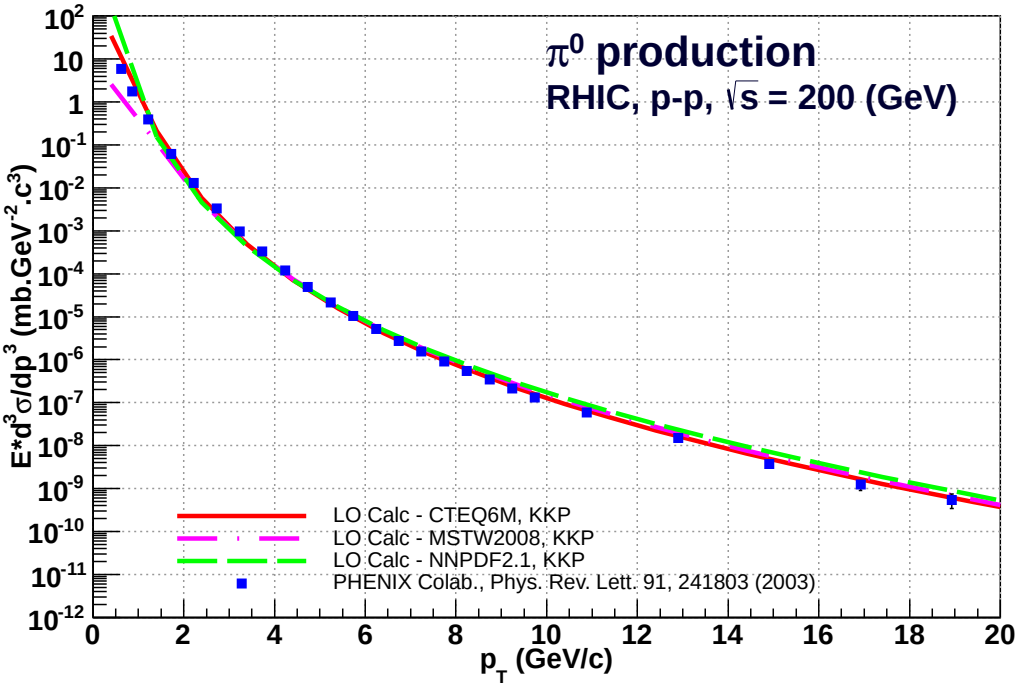

Figure 2.8: Comparison of the CTEQ6 [20], MSTW2008 [21] and NNPDF2.1 [22] parton distribution functions at the RHIC energies $\sqrt{s} = 200\,\text{GeV}$ for π^0 production.

Kretzer provides fragmentation into pions, kaons and charged hadrons in LO and NLO for $n_f = 5$ with restrictions $0.01 < x < 1$ for the Bjorken x and $0.8 < Q^2 < 10^6$ GeV^2 for the scale.

The combination of NNPDF2.1 and KKP parameterizations will be used from this point.

2.7 Intrinsic transverse momentum

As published in [7,26] the collinear approximation in the parton model is successful in the description of high-p_T particle production in pp collisions with the c.m. system energy $\sqrt{s} > 50\,\text{GeV}$ and for the p_T region $p_T \gtrsim 7\,\text{GeV/c}$. Because of non-perturbative effects for small p_T which the collinear approximation does not describe completely, the intrinsic transverse momentum (called k_T smearing) of a parton was included.

This effect is analogous to the Fermi motion of nucleons in a nucleus and can lead to a

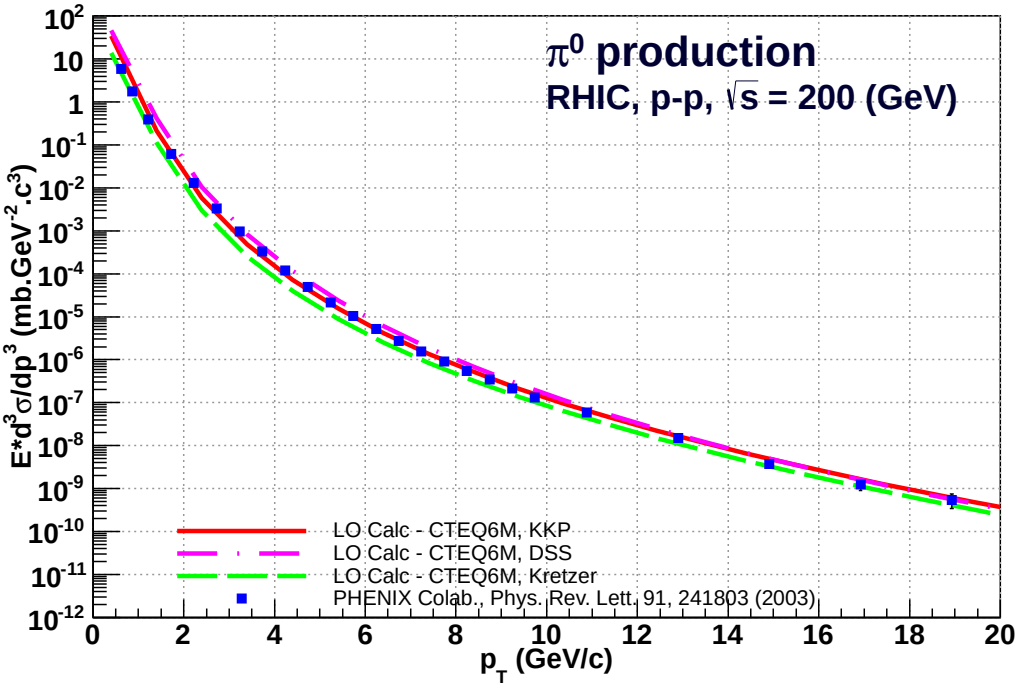

Figure 2.9: Comparison of the KKP [24], DSS [25] and Kretzer [5] parton fragmentation functions at the RHIC energies $\sqrt{s} = 200\,\mathrm{GeV}$ for π^0 production.

smearing of the p_T spectra. The k_T smearing function is a phenomenological parametrization and has been extracted from measurements of dimuon, diphoton and dijet pairs. This effect was investigated in [7, 15, 27–33].

The k_T smearing can be added into the calculation by a reformulation of the parton distribution as

$$dx_a\, f_{a/A}(x_a, Q) \to dx_a\, d^2k_{aT}\, g_N(k_{Ta}, Q^2)\, f_{a/N}(x_a, Q^2). \tag{2.35}$$

The inclusive invariant cross section for hadron production will be then given by

$$\begin{aligned} E\frac{d^3\sigma}{d^3p}\,(AB \to h\ X) \;=\; & K \sum_{abcd} \int dx_a dx_b dz_c d^2k_{Ta} d^2k_{Tb} g_p(k_{Ta}, Q^2) g_p(k_{Tb}, Q^2) f_{a/A}(x_a, Q^2) \\ & \times f_{b/B}(x_b, Q^2) D_{h/c}(z_c, \mu_F^2) \frac{\hat{s}}{\pi z_c^2} \frac{d\sigma}{d\hat{t}}\,(ab \to cd)\delta(\hat{s} + \hat{t} + \hat{u}) \end{aligned} \tag{2.36}$$

and the momentum fractions can be defined as

$$x_a = \frac{E_a + p_{la}}{\sqrt{s}}\,, \quad x_b = \frac{E_b - p_{lb}}{\sqrt{s}}\,, \tag{2.37}$$

where p_l is a longitudinal momentum in the beam direction. Then from four-momentum vectors $p_a = (E_a, \mathbf{k}_{Ta}, p_{\shortparallel a})$ and $p_b = (E_b, \mathbf{k}_{Tb}, p_{\shortparallel b})$ with

$$E_a = \frac{k_{Ta}^2}{2\sqrt{s}x_a} + \frac{x_a\sqrt{s}}{2}, \quad p_{\shortparallel a} = \frac{x_a\sqrt{s}}{2} - \frac{k_{Ta}^2}{2\sqrt{s}x_a} \tag{2.38}$$

and

$$E_b = \frac{k_{Tb}^2}{2\sqrt{s}x_b} + \frac{x_b\sqrt{s}}{2}, \quad p_{\shortparallel b} = \frac{k_{Tb}^2}{2\sqrt{s}x_b} - \frac{x_b\sqrt{s}}{2} \tag{2.39}$$

Mandelstam variables can be expressed. By the same definition as in (2.21) the Mandelstam variable $\hat{s}$ takes the form

$$\hat{s} = x_a x_b s + \frac{k_{Ta}^2 k_{Tb}^2}{x_a x_b s} - 2\mathbf{k}_{Ta} \cdot \mathbf{k}_{Tb}. \tag{2.40}$$

It is very useful to use the polar coordinates

$$d^2k_T \to dk_T\, d\phi\, J(k_T, \phi), \tag{2.41}$$

where $J(k_T, \cos\phi)$ is a Jacobian in the form

$$J(k_T, \phi) = k_T. \tag{2.42}$$

After that, the $\hat{s}$ variable takes the form

$$\hat{s} = x_a x_b s + \frac{k_{Ta}^2 k_{Tb}^2}{x_a x_b s} - 2k_{Ta}k_{Tb}\left(\cos\phi_a \cos\phi_b + \sin\phi_a \sin\phi_b\right). \tag{2.43}$$

Similarly, $\hat{t}$ and $\hat{u}$ Mandelstam variables can be expressed as

$$\hat{t} = -\frac{p_T}{z_c}\left(x_a\sqrt{s}e^{-y} + \frac{k_{Ta}^2}{\sqrt{s}\,x_a}\,e^{y} - 2k_{Ta}\cos\phi_a\right) \tag{2.44}$$

and

$$\hat{u} = -\frac{p_T}{z_c}\left(x_b\sqrt{s}e^{y} + \frac{k_{Tb}^2}{\sqrt{s}\,x_b}\,e^{-y} - 2k_{Tb}\cos\phi_b\right). \tag{2.45}$$

From [7, 15, 27–32, 34] implies that the transverse momentum distribution is best described by the Gaussian distribution

$$g_N(k_T, Q^2) = \frac{1}{\pi\langle k_T^2\rangle_N}\, e^{-k_T^2/\langle k_T^2\rangle_N}. \tag{2.46}$$

This Gaussian distribution introduces new non-perturbative parameter $\langle k_T^2\rangle$ - the mean intrinsic transverse momentum. The value of this parameter was chosen as in [15, 32]

$$\langle k_T^2\rangle_N(Q^2) = 1.2(\mathrm{GeV}^2) + 0.2\,\alpha_S(Q^2)Q^2 \tag{2.47}$$

as a function of square of momentum transfer Q^2 and where N denotes nucleon.

Moreover, similarly as in (2.25) to (2.28), the integration over z_c can be performed using a delta function with

$$z_c = \frac{p_T}{\hat{s}} \left[\sqrt{s} \left(x_a e^{-y} + x_b e^{y} \right) + \frac{1}{\sqrt{s}} \left(\frac{k_{Ta}^2}{x_a} e^{y} + \frac{k_{Tb}^2}{x_b} e^{-y} \right) - 2 \left(k_{Ta} \cos\phi_a + k_{Tb} \cos\phi_b \right) \right] \tag{2.48}$$

and applying boundary conditions $z_c \leq 1$ on Eq. 2.48 leads to the quadratic equation for $x_{b\,min}$. The results for $x_{b\,min}$ is then

$$\begin{aligned} x_{b\,min} = e^{-y}(&-e^{2y}\, k_{Ta}^2\, p_T \sqrt{s} - p_T\, s^{3/2}\, x_a^2 - 2e^{2y} s\, x_a (k_{Ta}\, k_{Tb} (\cos\phi_a \cos\phi_b \\ &+ \sin\phi_a \sin\phi_b) - p_T (k_{Ta}\, \cos\phi_a + k_{Tb}\, \cos\phi_b)) \\ &\pm (4\, e^{y}\, k_{Tb}^2\, s^{3/2}\, x_a (e^{y}\, p_T - \sqrt{s}\, x_a)(e^{y}\, k_{Ta}^2 - p_T \sqrt{s}\, x_a) + p_T\, s^{3/2}\, x_a^2 \\ &+ 2\, e^{y}\, s\, x_a (k_{Ta}\, k_{Tb} (\cos\phi_a \cos\phi_b + \sin\phi_a \sin\phi_b) \\ &- p_T (k_{Ta}\, \cos\phi_a + k_{Tb}\, \cos\phi_b)))^{1/2}) \,/\, (2\, s^{3/2}\, x_a\, (e^{y}\, p_T - \sqrt{s}\, x_a)) \end{aligned} \tag{2.49}$$

and by applying the other condition $x_{b\,min} \leq 1$ same roots of quadratic equations are obtained for both roots of $x_{a\,min}$

$$\begin{aligned} x_{a\,min} = (&k_{Tb}^2\, p_T \sqrt{s} + e^{2y}\, p_T\, s^{3/2} + 2\, e^{y}\, s (k_{Ta}\, k_{Tb} (\cos\phi_a \cos\phi_b \\ &+ \sin\phi_a \sin\phi_b) - p_T (k_{Ta}\, \cos\phi_a + k_{Tb}\, \cos\phi_b)) \\ &\pm (4\, e^{y}\, k_{Ta}^2\, s^{3/2} (e^{y} \sqrt{s} - pT)(e^{y}\, p_T \sqrt{s} - k_{Tb}^2) + s (k_{Tb}^2\, p_T \\ &+ 2\, e^{y} (k_{Ta}\, k_{Tb} (\cos\phi_a \cos\phi_b + \sin\phi_a \sin\phi_b) \\ &- p_T (k_{Ta}\, \cos\phi_a + k_{Ta}\, \cos\phi_b)))^2)^{1/2}) \,/\, (2\, e^{y}\, s^2 - 2\, p_T\, s^{3/2}). \end{aligned} \tag{2.50}$$

Finally, restrictions on the initial transverse momentum $k_{Ta} < x_a \sqrt{s}$ and $k_{Tb} < x_b \sqrt{s}$ can be obtained. In some cases, some of Mandelstam variables can approach zero, if the initial k_T is too large. That is a problem for the partonic cross section which could then diverge. This problem is solved by adding a regularization mass μ^2 to denominators of the partonic cross sections with the value $\mu = 0.8\,\mathrm{GeV}$ for quarks and $\mu = 0.2\,\mathrm{GeV}$ for gluons as in [15].

It is expected that the k_T smearing leads to an increase of the cross section as discussed in [7].

2.8 Analysis and results

For the following calculations number of flavours $n_f = 4$ was used. All calculations are presented for $p_T \geq 2$ GeV/c. For $p_T < 2$ GeV/c it is necessary to combine QCD hard processes and soft particle production. Calculations for low p_T can be done using e.g. HIJING [35] or Pythia [36] which include models that contain the string model for soft particle production.

In correspondence with [22] the value of Λ_{QCD} fundamental constant was chosen as $\Lambda_{QCD} = 0.326\,\text{GeV}$ for the number of flavours $n_f = 4$. Next, $Q = p_T$ was chosen as a scale of the parton distribution function and $\mu_F = p_T/z_c$ for the fragmentation momentum scale.

In this work the extraction of the K-factor from data for each $\sqrt{s}$ is based on minimizing the χ^2:

$$\chi^2 = \sum_i^N \left(\frac{K\sigma_i^{calc} - \sigma_i^{exp}}{\sigma_i^{exp}} \right)^2, \tag{2.51}$$

where the sum runs over the transverse momenta p_T, σ_i^{exp} is the measured cross section for p_{Ti} and σ_i^{calc} is the calculated cross section for p_{Ti} without the K-factor. The error of the K-factor ΔK is estimated as the standard deviation in the form

$$\Delta K = \sqrt{\frac{1}{N-1} \sum_i^N \left(\frac{\sigma_i^{calc}}{\sigma_i^{exp}} - K \right)^2}. \tag{2.52}$$

For the evaluation the inclusive cross section several integration methods were used. For integrals with constant limits of integration adaptive multidimensional integration (cubature) method of vector-valued integrands over hypercubes `adapt` [37] was used. For other integrals 1D globally adaptive integrator using Gauss-Kronrod quadrature subroutine `dqag` from the QUADPACK [38] was used.

Final results for inclusive high-p_T particle production invariant differential cross section are plotted in the Figures 2.10 - 2.17. These results were calculated for c.m. energies $\sqrt{s} = 31.56$, 62, 200, 900, 2760 and 7000 GeV in mid-rapidity as a function of the transverse momenta. On the top part of figures, results for the collinear parton model are plotted with the green dashed line, for the parton model with k_T smearing with solid red line. Experimental data are denoted by blue squares. On the bottom part, ratios data-to-theory are plotted as a function of the transverse momentum.

By comparing the data and theory in the Figures 2.10 - 2.17 it is found that for high-p_T about $\gtrsim 5\,\text{GeV/c}$ both models give same results, but for smaller p_T model with the k_T smearing describes the data better.

$\sqrt{s}$ [GeV]	Experiment	Ref.	Syst.err.	Produced particles	K	ΔK	χ^2
31.56	E706	[39]	15%	π^0	5.56	1.33	0.58069
62	PHENIX	[40]	19%	π^0	5.49	2.22	0.73374
200	Star	[41]	12%	π^0	3.06	0.59	0.25008
200	PHENIX	[42]	9.6%	π^0	3.08	1.08	1.16019
900	Alice	[43]	2.4%	π^0	1.08	0.23	0.29919
2760	Alice	[43]	7%	π^0	0.75	0.03	0.03691
2760	CMS	[44]		$h^+ + h^-$	0.78	0.14	0.32416
7000	Alice	[43]	7%	π^0	0.46	0.10	0.55305

Table 2.2: Results of the K-factor for the collinear parton model. The K-factors were obtained by minimizing χ^2 as in Eq. (2.51). Errors of the K-factor are computed from Eq. (2.52). Systematic error is not included in the estimation of ΔK. Notice that the K-factor is obtained with the NNPDF2.1 [22] and KKP [24] parton distribution and fragmentation function with the scale $Q = p_T$ and $\mu_F = p_T/z_c$.

Results of the K-factor, its errors (systematic errors are not included) and values of χ^2 for collinear parton model are summarized in Table 2.2. In Table 2.3 results for parton model with k_T smearing are presented. Both tables contain reference and systematic error (if known) for the experimental data.

For energies $\sqrt{s} > 900$ GeV the K-factor becomes less then one. It means that the calculated cross section is bigger then the measured cross section. This is consistent with e.g. NLO prediction in [43].

K-factors obtained for different energies are plotted in Fig. 2.18. Error bars correspond to the statistical error ΔK computed from Eq. (2.52). Obtained K-factors decrease systematically with increasing $\sqrt{s}$. Computed K-factors, except for the K-factor for $\sqrt{s} = 31.56$ GeV, are in good agreement with calculated K-factors in [45].

$\sqrt{s}$ [GeV]	Experiment	Ref.	Syst.err.	Produced particles	K	ΔK	χ^2
31.56	E706	[39]	15%	π^0	1.60	0.61	1.49197
62	PHENIX	[40]	19%	π^0	5.03	0.83	0.23528
200	Star	[41]	12%	π^0	2.41	0.61	0.43005
200	PHENIX	[42]	9.6%	π^0	2.22	0.34	0.39273
900	Alice	[43]	2.4%	π^0	0.81	0.16	0.23136
2760	Alice	[43]	7%	π^0	0.62	0.06	0.06136
2760	CMS	[44]		$h^+ + h^-$	0.74	0.09	0.17869
7000	Alice	[43]	7%	π^0	0.44	0.09	0.48485

Table 2.3: Results of the K-factor for the parton model with k_T smearing. The K-factors were obtained by minimizing χ^2 as in Eq. (2.51). Errors of the K-factor are computed from Eq. (2.52). Systematic error is not included in the estimation of ΔK. Notice that the K-factor is obtained with the NNPDF2.1 [22] and KKP [24] parton distribution and fragmentation function with the scale $Q = p_T$ and $\mu_F = p_T/z_c$.

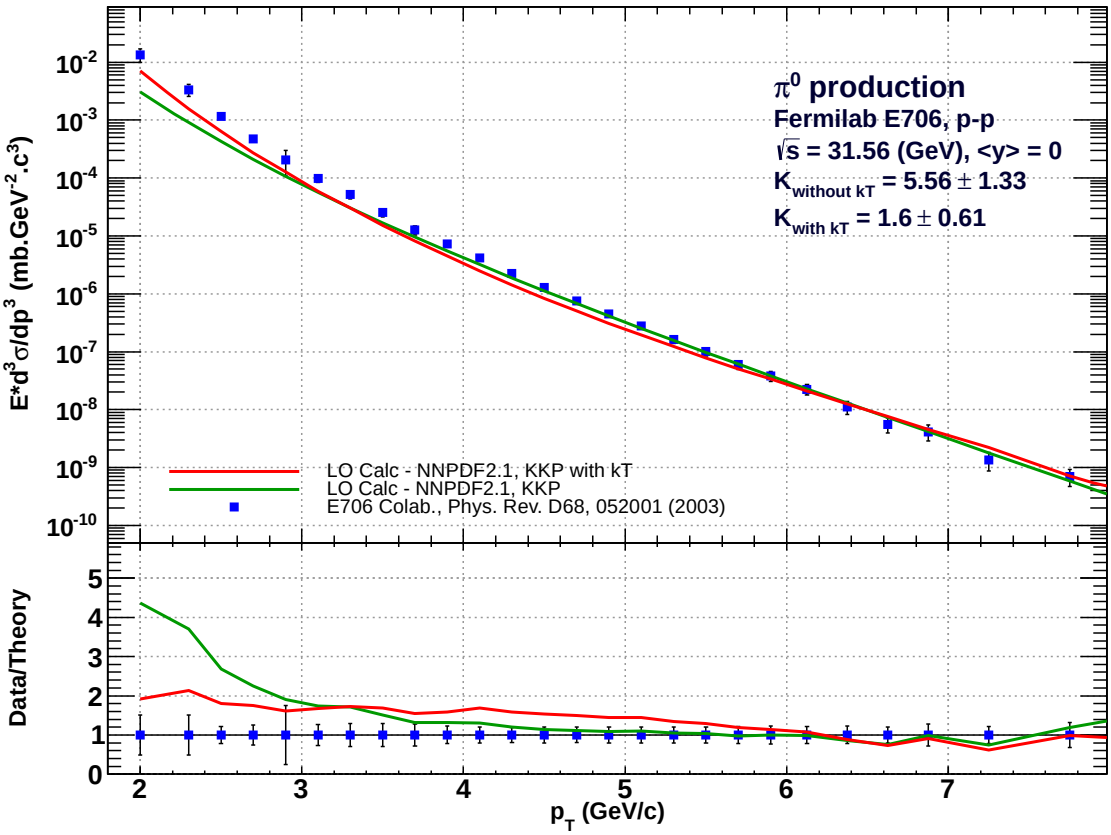

Figure 2.10: **Top**: Inclusive cross section for π^0 production in pp collisions at $\sqrt{s} = 31.56$ GeV at mid-rapidity. Data are from experiment E706 [39]. **Bottom**: The ratios data-to-theory as a function of transverse momentum p_T.

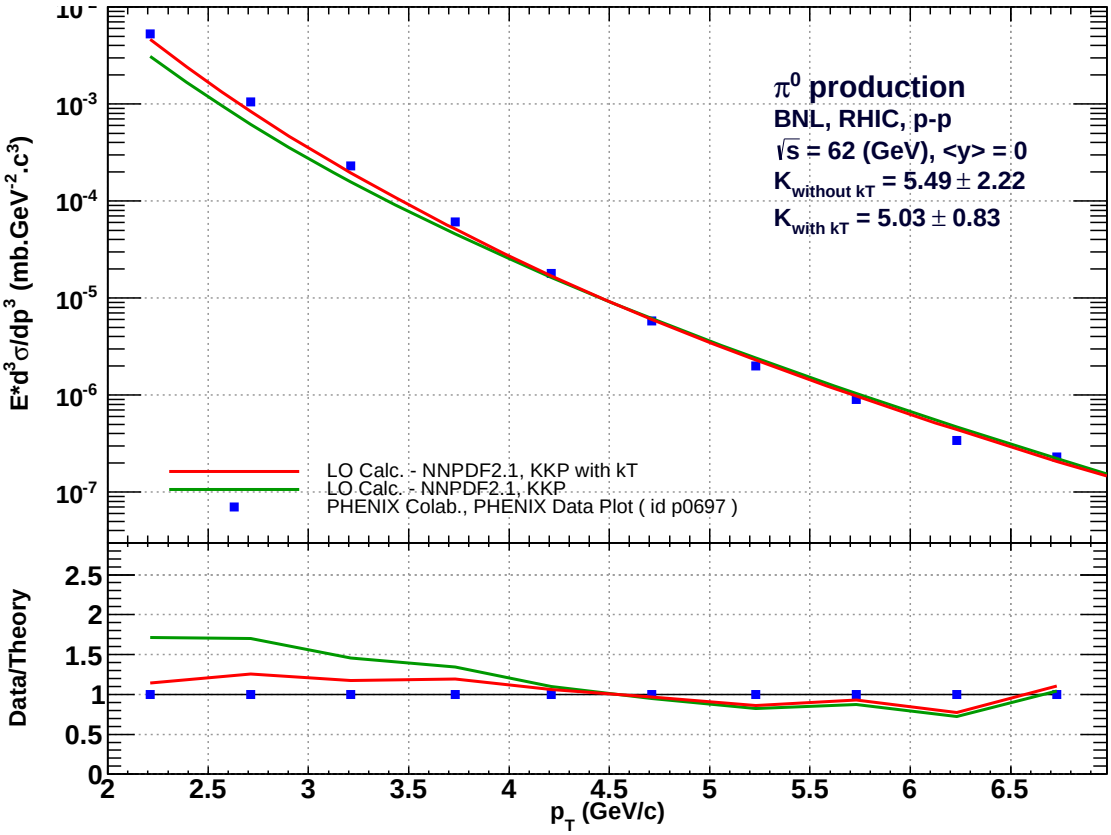

Figure 2.11: **Top**: Inclusive cross section for π^0 production in pp collisions at $\sqrt{s} = 62$ GeV at mid-rapidity. Data are from experiment PHENIX [40]. **Bottom**: The ratios data-to-theory as a function of transverse momentum p_T.

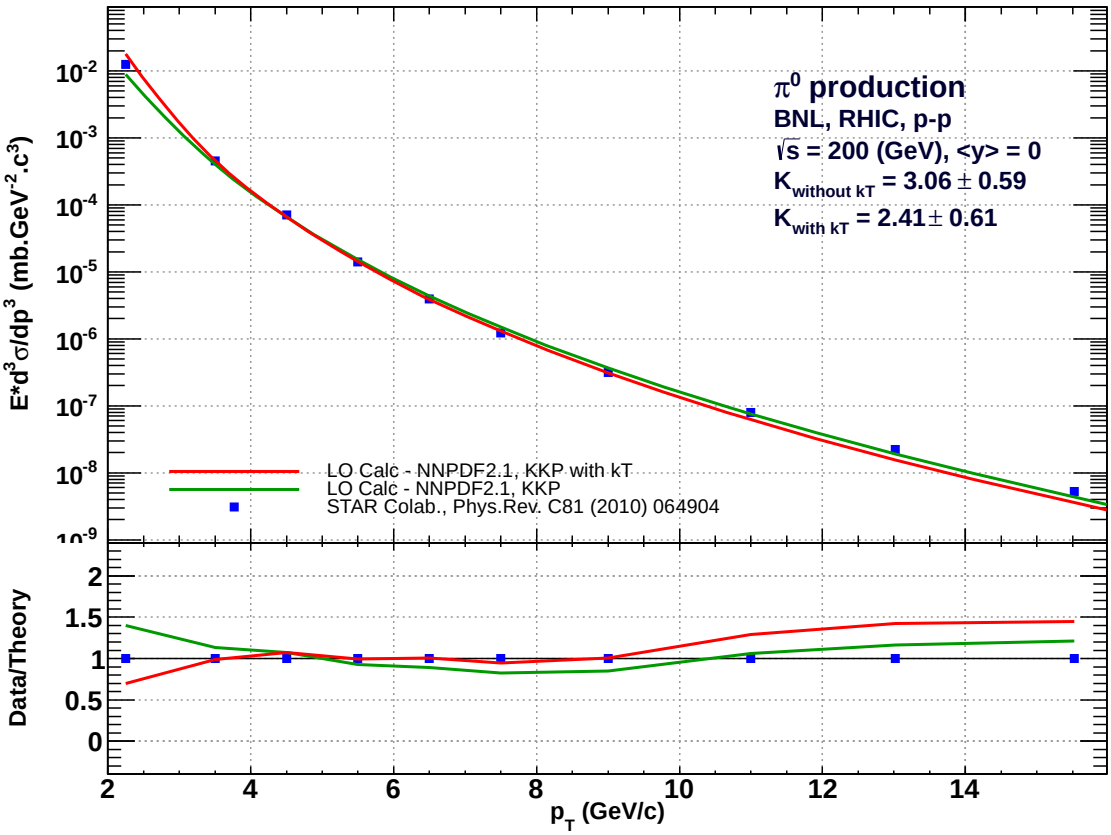

Figure 2.12: **Top**: Inclusive cross section for π^0 production in pp collisions at $\sqrt{s} = 200$ GeV at mid-rapidity. Data are from experiment STAR [41]. **Bottom**: The ratios data-to-theory as a function of transverse momentum p_T.

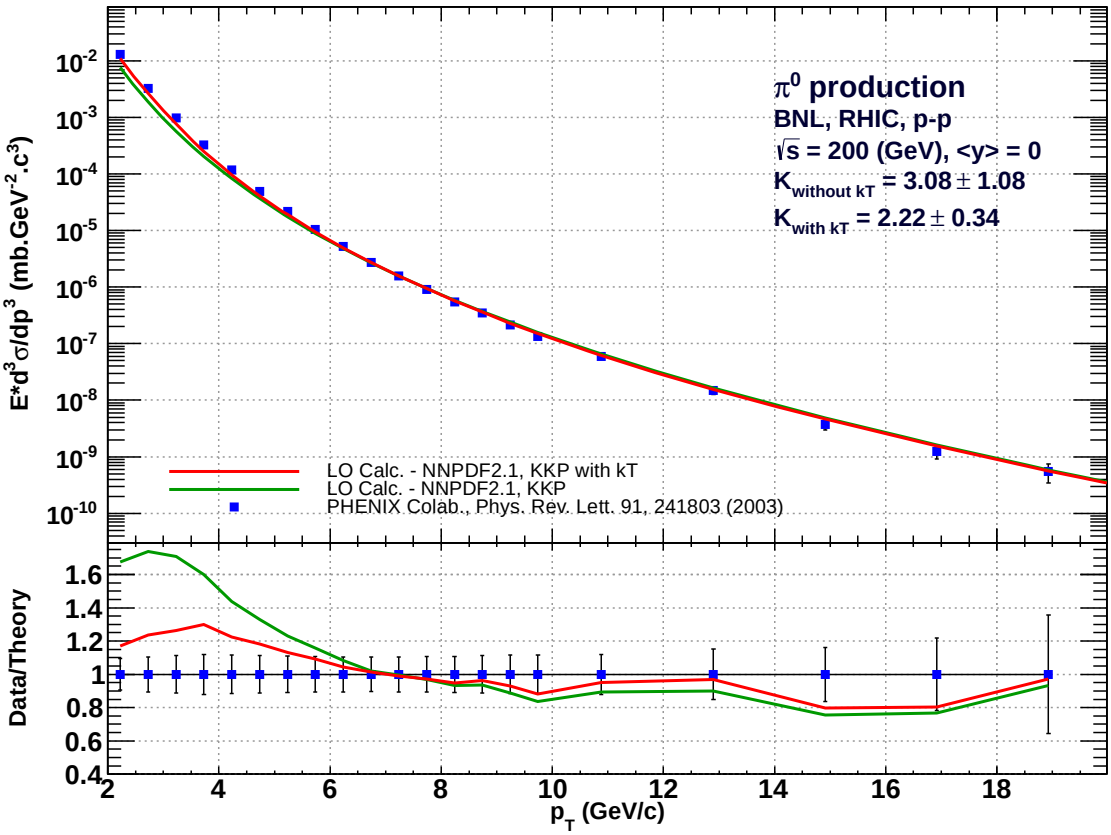

Figure 2.13: **Top**: Inclusive cross section for π^0 production in pp collisions at $\sqrt{s} = 200$ GeV at mid-rapidity. Data are from experiment PHENIX [42]. **Bottom**: The ratios data-to-theory as a function of transverse momentum p_T.

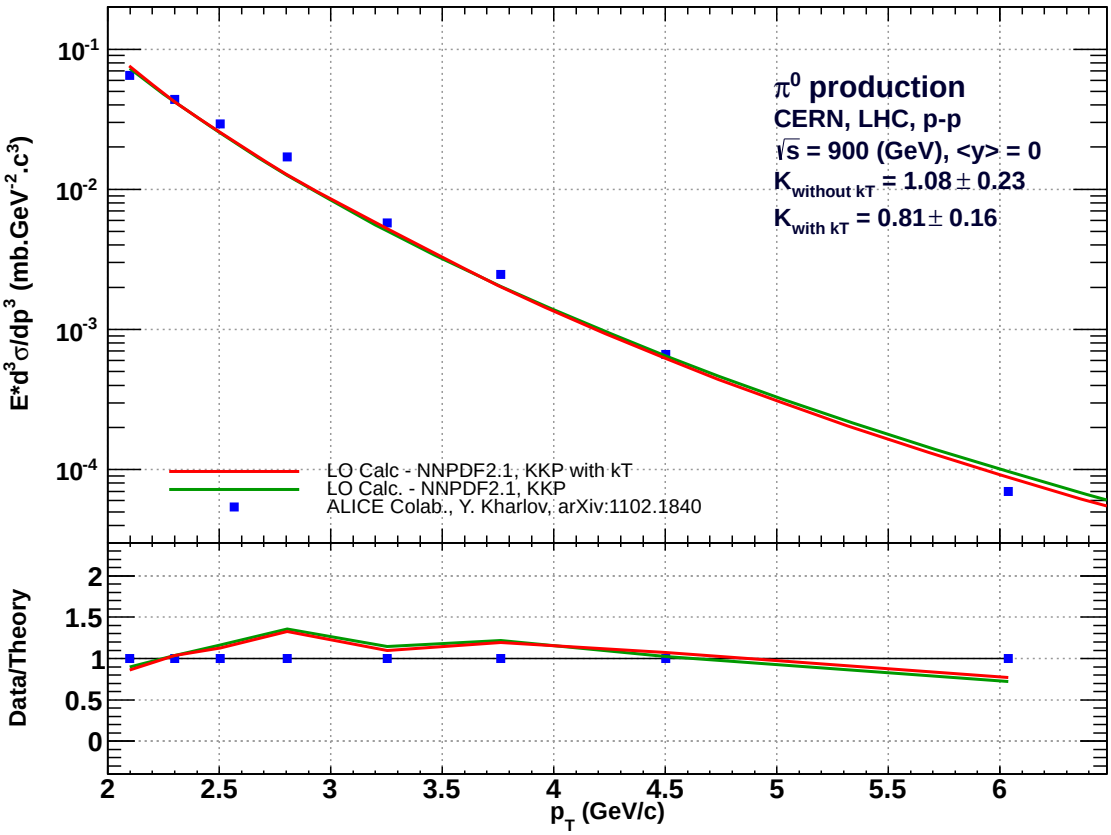

Figure 2.14: **Top**: Inclusive cross section for π^0 production in pp collisions at $\sqrt{s} = 900$ GeV at mid-rapidity. Data are from experiment ALICE [43]. **Bottom**: The ratios data-to-theory as a function of transverse momentum p_T.

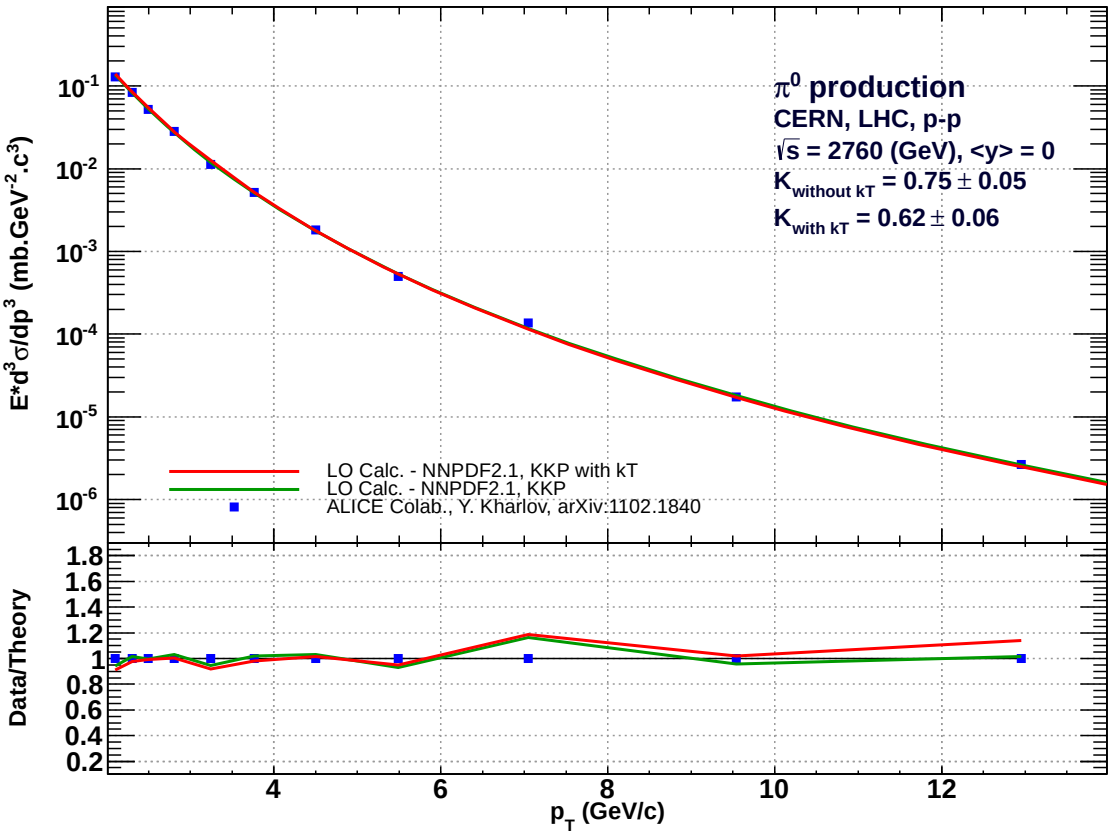

Figure 2.15: **Top**: Inclusive cross section for π^0 production in pp collisions at $\sqrt{s} = 2760$ GeV at mid-rapidity. Data are from experiment ALICE [43]. **Bottom**: The ratios data-to-theory as a function of transverse momentum p_T.

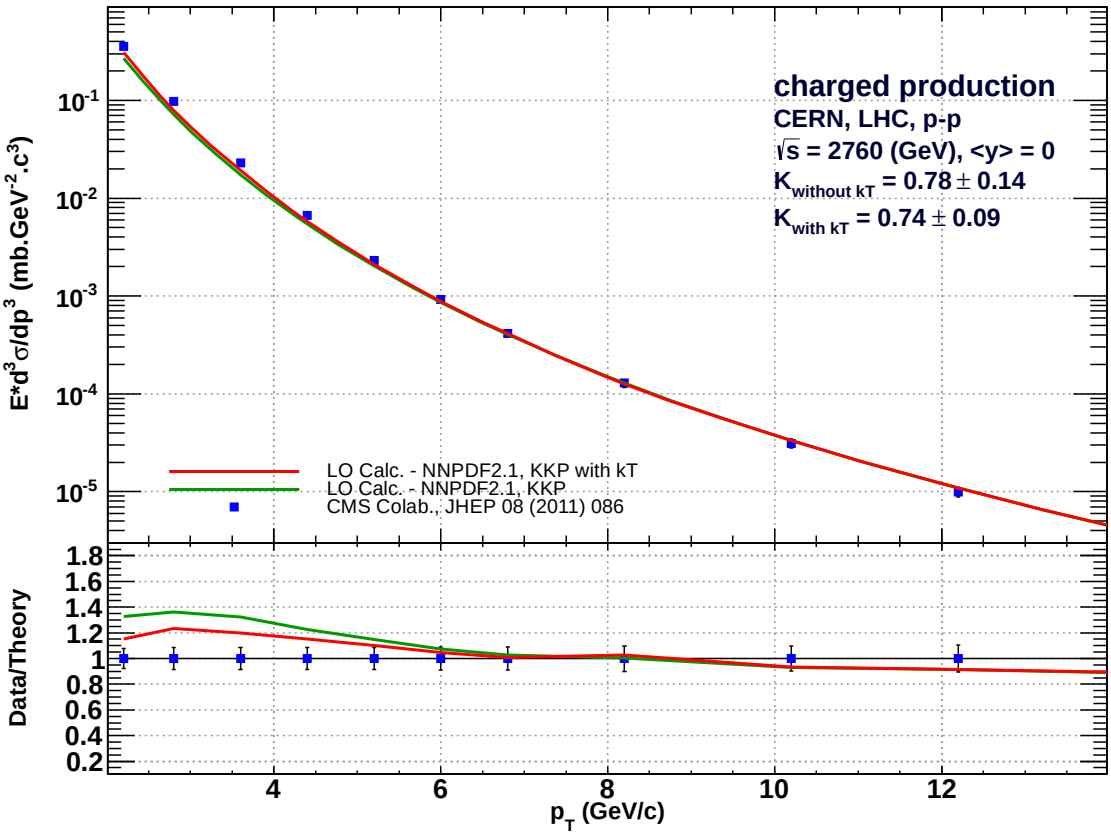

Figure 2.16: **Top**: Inclusive cross section for charged hadrons production $(h^+ + h^-)$ in pp collisions at $\sqrt{s} = 2760$ GeV at mid-rapidity. Data are from experiment CMS [44]. **Bottom**: The ratios data-to-theory as a function of transverse momentum p_T.

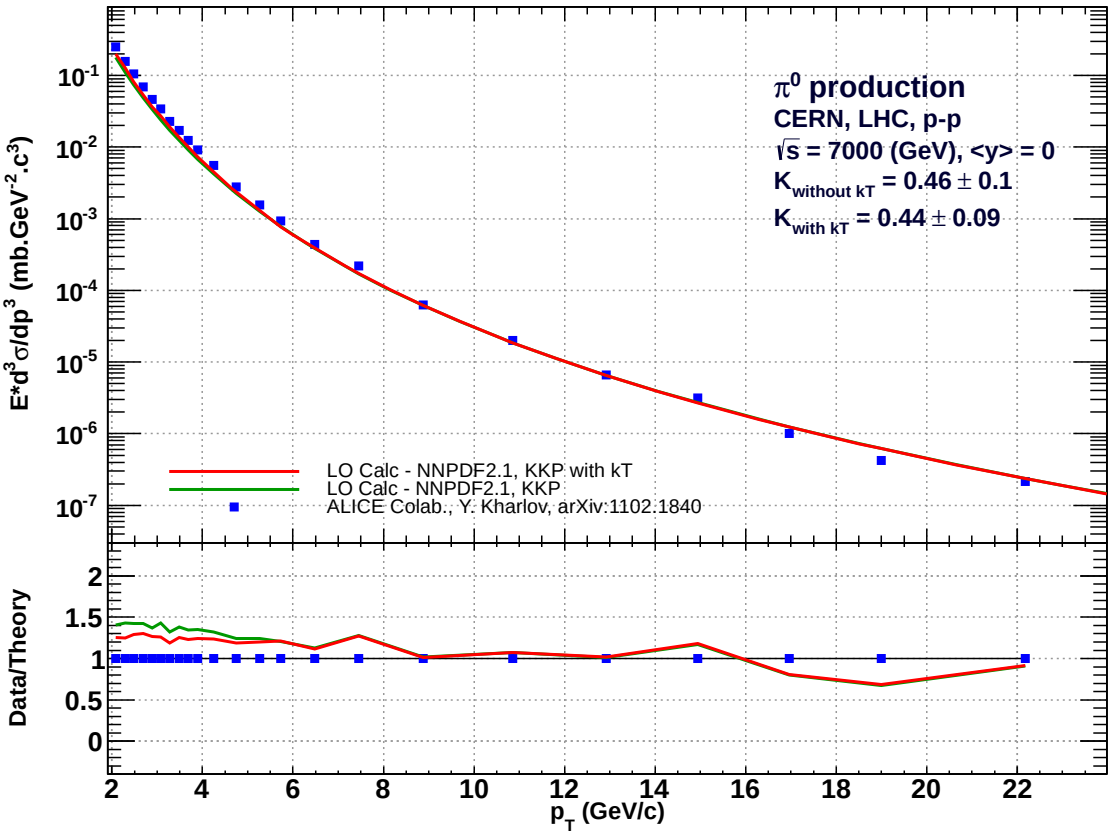

Figure 2.17: **Top**: Inclusive cross section for π^0 production in pp collisions at $\sqrt{s} = 7000$ GeV at mid-rapidity. Data are from experiment ALICE [43]. **Bottom**: The ratios data-to-theory as a function of transverse momentum p_T.

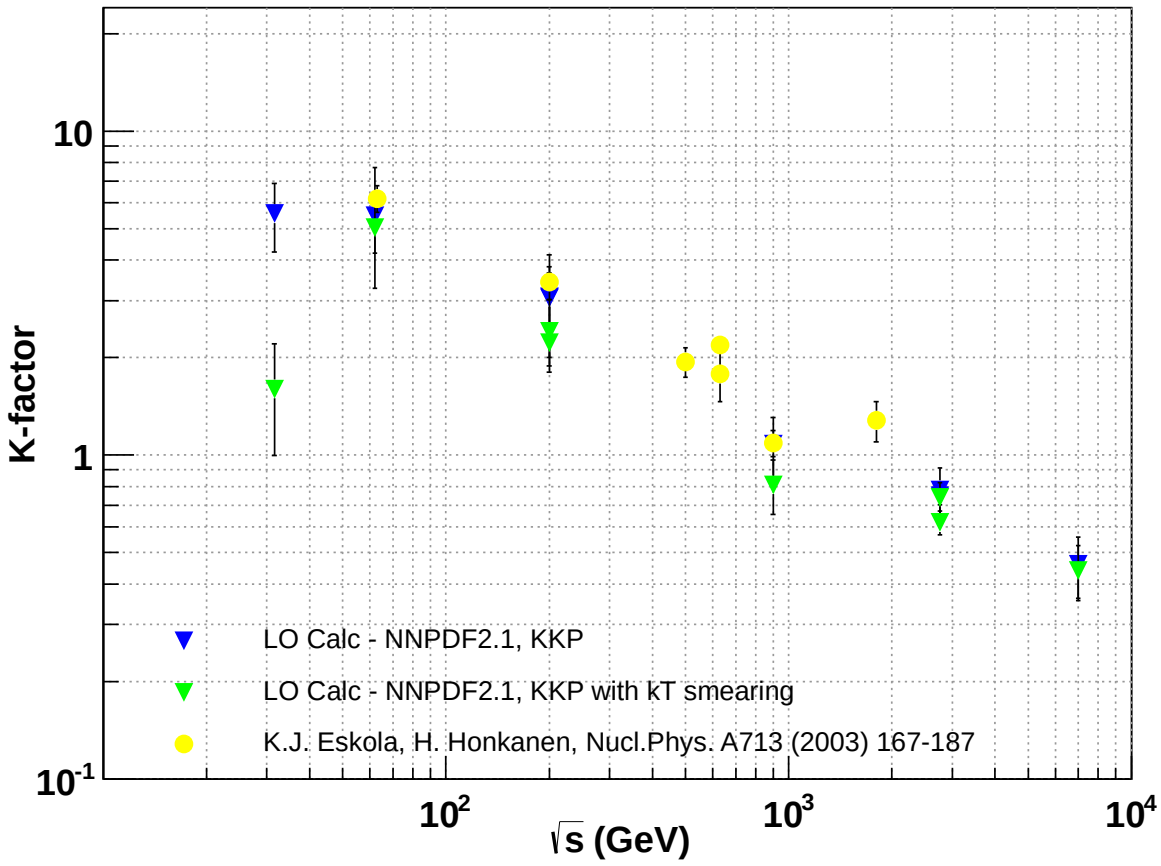

Figure 2.18: The K-factors plotted as a function of $\sqrt{s}$ for $\sqrt{s} = 31.56$, 62, 200, 900, 2760, 7000 GeV for π^0 and charged particles production. The error bars correspond to the statistical error ΔK computed from (2.52) (systematic error is not included). Obtained K-factors are compared with K-factors from K. J. Eskola and H. Honkanen [45].

Chapter 3

Nucleon-nucleus collisions

The proton-nucleus (pA) collision are much more complicated than proton-proton collision. Experimentally it was found that particle spectra in pA collision has a different shape than inclusive spectra in pp collisions. In a collision with nucleus, especially with heavy one, we expect multiple soft scattering before the hard scattering. It was found that the passage of parton through the nuclear matter manifests number of effects, for example the Cronin effect, shadowing or saturation.

The proton-nucleus collisions also offer an opportunity to study small-x physics, to determine nuclear modification factors and nuclear parton distribution functions (nPDF), to study ultra-peripheral collisions (UPC) and to provide support for heavy-ion collisions, where pA collisions could be essential for the interpretation of heavy-ion results. More information can be found e.g. in [46].

The Cronin effect is an effect of an increase of the pA cross section compared to scaled pp cross section in transverse momentum region $3 \lesssim p_T \lesssim 6\,\mathrm{GeV/c}$. The Cronin effect was first measured in 1979 [47] in Fermilab Proton Area.

3.1 Inclusive cross section

The extended QCD improved quark-parton model in the form of Eq. 3.1 was used. This model is based on one hard scattering in pA collisions. Effects of soft scattering of the parton before the hard scattering are hidden in the initial transverse momentum so-called k_T-broadening. The following formula for the inclusive differential cross section (minimum-biased) has the form

$$E\frac{d^3\sigma_{pA}}{dp^3}\,(p\,A\to h\;X) \;=\; K\sum_{abcd}\int d^2b\,t_A(b)\int dx_a\,dx_b\,dz_c\,d^2k_{Ta}\,d^2k_{Tb}\,g_A(k_{Ta},Q^2,b)$$
$$\times g_p(k_{Tb},Q^2)\,f_{a/p}(x_a,Q^2)\,f_{b/A}(b,x_b,Q^2)$$
$$\times D_{h/c}(z_c,\mu_F^2)\frac{1}{\pi z_c}\,\frac{d\sigma}{d\hat{t}}\,(ab\to cd), \tag{3.1}$$

where an integral over the impact parameter b was added, $t_A(b)$ is the nuclear thickness function and $f_{b/A}(b,x_b,Q^2)$ is the parton distribution per nucleon inside the nucleus and is discussed in more detail in the next section.

The nuclear thickness function or nuclear profile function $t_A(b)$ gives the number of nucleons in the nucleus A per unit area along a direction z separated from the center of the nucleus by an impact parameter b

$$t_A(b)=\int dz\,\rho(b,z), \tag{3.2}$$

where $\rho(b,z)$ is a parametrization of the distribution normalized to the number of nucleons A

$$\int d^2b\,t_A(b)=A. \tag{3.3}$$

In this work the two-parameter Fermi model (2pF) (also known as Wood-Saxon distribution) was chosen as the parametrization of ρ in the form

$$\rho(r)=\frac{\rho_0}{1+e^{\frac{r-c}{z}}} \tag{3.4}$$

where $r=\sqrt{b^2+z^2}$, ρ_0 is determined by the normalization in Eq. (3.3) and c and z are two model parameters.

Values of parameters for two-parameter Fermi model from [48] used in this work are in Table 3.1.

Nucleus	$\langle r^2\rangle^{1/2}$ [fm]	c [fm]	a [fm]
^{184}W	5.40(4)	6.51(7)	0.535(36)
^{197}Au	5.33(5)	6.38(6)	0.535(27)
^{207}Pb	5.513(32)	6.62(6)	0.546(10)

Table 3.1: The values of parameters for two-parameter Fermi model for selected nuclei from [48].

3.2 Nuclear modification factor

The determination of the parton momentum fraction inside the nucleus is more difficult because of many effects e.g. shadowing, anti-shadowing, EMC effect or Fermi motion as shown in the Figure 3.1. These effects have been firstly studied by comparing structure function measured on bound nucleons and on deuterium (as the best approximation to the structure function of free nucleon) on the lepton-nucleus DIS processes. The R_i^A in Fig. 3.1 is defined as ratio F_2^A/F_2^D of distribution functions as a function of x.

There for $x < 0.05 - 0.1$ the ratio F_2^A/F_2^D is smaller than unity and it is called "shadowing". For $x \approx 0.1 - 0.2$ the ratio is larger than one by a few percent, this behavior is called "anti-shadowing". Region $0.1 - 0.2 < x < 0.6$ is known as the "EMC effect". EMC effect reaches a minimum around $x = 0.6$. The "Fermi motion" region is for $x > 0.8$ where the ratio grows above unity. For a detail review, see [49].

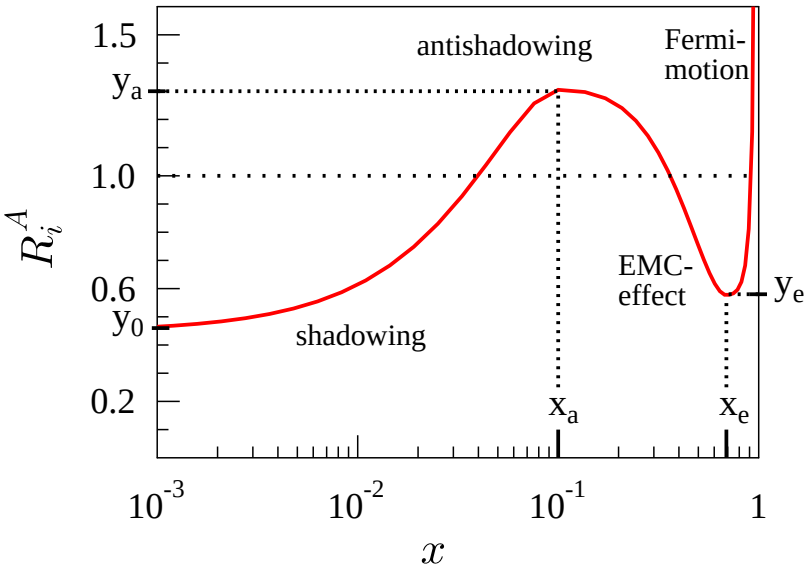

Figure 3.1: An illustration of the fit function R_i^A with the outlining of the effects. Picture is from [50].

There are two ways how to get the parton distribution functions in a nucleus. Either, the nuclear parton distribution function (nPDF) can be used e.g. HKN07 [51], or nPDF is obtained using the nuclear modification factor R_f^A. The latter option has the benefit

that the classical parton distribution function can be used in the form

$$f_{b/A}(x_b, Q^2) = R_f^A(x_b, Q) \left[\frac{Z}{A} f_{a/p}(x, Q^2) + \left(1 - \frac{Z}{A}\right) f_{a/n}(x, Q^2) \right], \tag{3.5}$$

where $R_f^A(x_b, Q)$ is the nuclear modification factor (depends the parton flavour and parton momentum fraction x_b), A is the number or nucleons and Z is the number of protons in the nucleus. Factors Z/A and $(1 - Z/A)$ are here because of the isospin effects. Finally, $f_{a/n}$ is the parton distribution function of the neutron (compared to the proton the valence u and d quarks are different).

The nuclear modification factor $R_f^A(x_b, Q)$ for each parton flavour f is defined as

$$R_f^A(x_b, Q) = f_f^A(x_b, Q^2) \,/\, f_f^p(x, Q^2), \tag{3.6}$$

where f_f^A is the nuclear parton distribution function and f_f^p is the classical parton distribution function. R_f^A is normalized to one nucleon.

The EKS98 (Eskola-Kolhinen-Salgado) [52] and the EPS09 (Eskola-Paukkunen-Salgado) [50] nuclear modification factors were used for the calculation in this work.

3.3 k_T broadening

The k_T broadening is an expression for high-energy parton propagating through a nuclear medium that experiences multiple soft scatterings and so increased its transverse momentum. It can be imagined as parton multiple gluonic exchanges with nucleons. The model of a $q\bar{q}$ dipole propagating described more in detail in [53] is used in this work for describing the k_T broadening.

The initial parton transverse momentum distribution of a projectile nucleon is changed by the k_T broadening as a function of the impact parameter b

$$g_A(k_T, Q^2, b) = \frac{1}{\pi \langle k_T^2 \rangle_A} e^{-k_T^2 / \langle k_T^2 \rangle_A}, \tag{3.7}$$

where

$$\langle k_T^2 \rangle_A(Q^2) = \langle k_T^2 \rangle_N(Q^2) + 2\, C\, t_A(b). \tag{3.8}$$

where $\langle k_T^2 \rangle_N(Q^2)$ is the same as in Eq. (2.47).

The factor C is calculated as

$$C = \left. \frac{d\sigma_{q\bar{q}}^N}{dr^2} \right|_{r=0}, \tag{3.9}$$

from the color dipole approximation cross section $\sigma_{q\bar{q}}^{N}$ at $r = 0$.The GBW (Golec-Biernat and Wusthoff) [54] parametrization was used in this work in the form

$$\sigma_{q\bar{q}}^{N}(x,r) = \sigma_0 \left(1 - e^{-\frac{r^2 Q_0^2}{4\left(\frac{x}{x_0}\right)^{\lambda}}} \right), \tag{3.10}$$

where x is the momentum fraction of the parton and parameters are $Q_0^2 = 1\,\mathrm{GeV}$, $\sigma_0 = 23.9\,\mathrm{mb}$, $x_0 = 0.0003$ and $\lambda = 0.287$.

The first derivative of (3.10) at $r = 0$ then yields

$$C = \frac{\sigma_0 Q_0^2}{4\left(\frac{x}{x_0}\right)^{\lambda}}. \tag{3.11}$$

3.4 Analysis and results

Same setting as for *pp* collision (see Sec. 2.8) was used in following calculations. It means that the number of flavours is $n_f = 4$, the parton distribution scale Q^2 was chosen as $Q = p_T$ and the fragmentation scale is $\mu_F = p_T/z_c$.

The K-factor was determined by minimizing the χ^2 Eq. (2.51) and its error was estimated by Eq. (2.52) (systematic error is not included). The nuclear parton distribution function was calculated by the combination of nuclear modification factors EPS09 [50] and the NNPDF2.1 [22] parton distribution function with $\Lambda_{QCD} = 0.326\,\mathrm{GeV}$ for $n_f = 4$.

Results for proton-tungsten collision for energy $E_{LAB} = 300$ and 400 GeV for production of charged $((\pi^+ + \pi^-)/2)$ pions are shown in Fig. 3.2 and 3.3. There results are compared with data from FNAL Proton Area [55]. Final results for the K-factor for proton-tungsten collision are summarized in the Table 3.2.

The predicted invariant inclusive cross section for π^0 production at $\sqrt{s} = 3500\,\mathrm{GeV}$ is presented in Fig. 3.5 where the K-factor 0.59 follows from the analysis in Sec. 2.8.

Nuclear modification factor R_{pA} was calculated for RHIC at $\sqrt{s} = 200\,\mathrm{GeV}$ and was predicted for LHC at $\sqrt{s} = 3500\,\mathrm{GeV}$. Nuclear modification factor R_{pA} is defined as

$$R_{pA} = \frac{\frac{d^3\sigma^{pA}}{dp^3}}{A\,\frac{d\sigma^{pp}}{dp^3}}, \tag{3.12}$$

where σ^{pA} is inclusive cross section for proton-nucleus collisions and σ^{pp} is inclusive cross section for proton-proton collisions.

Energy [GeV]	Ref.	Syst.err.	Produced particles	K	ΔK	χ^2
E_{LAB} =300	[55]	20%	$(\pi^+ + \pi^-)/2$	1.31	0.50	0.30902
E_{LAB} =400	[55]	20%	$(\pi^+ + \pi^-)/2$	1.84	0.82	0.69828
$\sqrt{s}$ =200	[56]		π^0	2.25	0.47	0.63296

Table 3.2: Results for the K-factor for the parton model with the k_T broadening. K-factors were obtained by minimizing χ^2 as in Eq. (2.51). Errors of the K-factor are computed from the Eq. (2.52). Systematic error is not included in the estimated for ΔK. Notice that the K-factor is obtained with the NNPDF2.1 [22] and KKP [24] parton distribution, fragmentation functions with the scale $Q = p_T$ and $\mu_F = p_T/z_c$ and with the nuclear modification factors EPS09 [50].

In Fig. 3.6 and 3.7 result for nuclear modification factor R_{pA} is plotted, where green solid line denote R_{pA} without EPS09 (which include other effects e.g. shadowing) and red solid line refer to R_{pA} with EPS09 (shadowing and other effect are included).

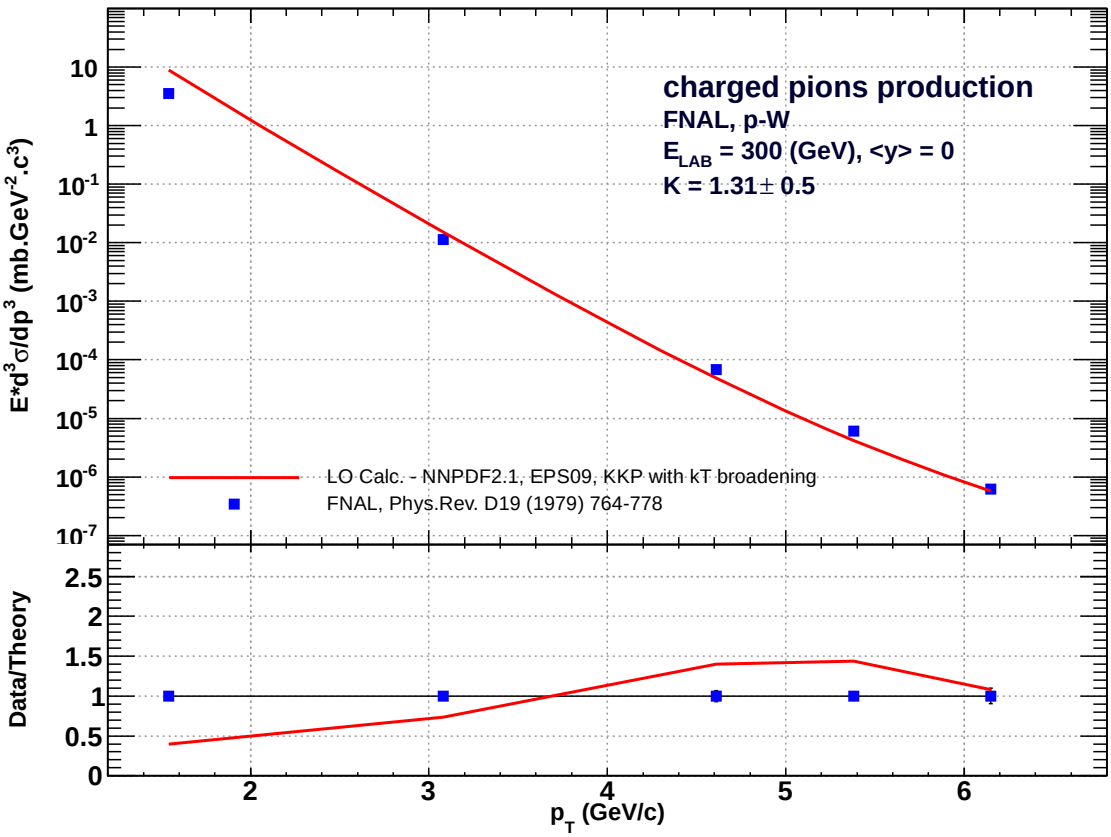

Figure 3.2: **Top**: Inclusive cross section for charged pions production $(\pi^+ + \pi^-)/2$ in proton-tungsten (pW) collision at $E_{LAB} = 300$ GeV at mid-rapidity. Data are from [55]. **Bottom**: The ratios data-to-theory as a function of transverse momentum p_T.

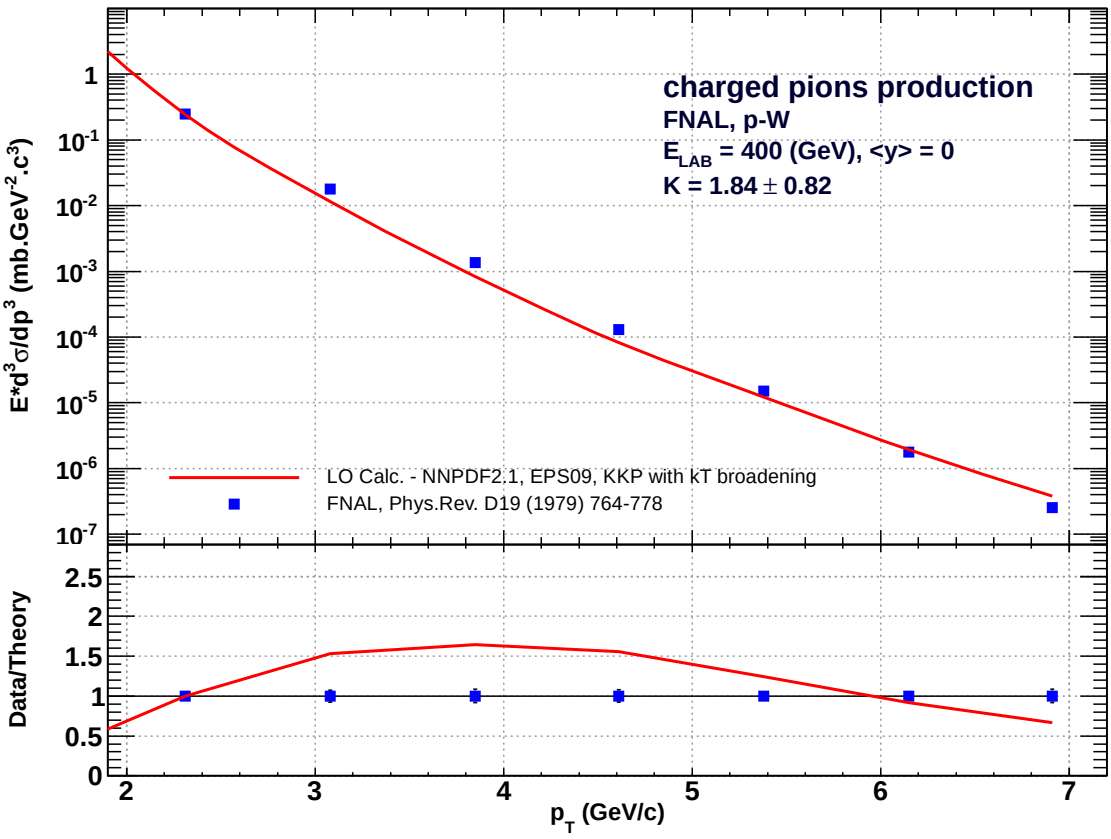

Figure 3.3: **Top**: Inclusive cross section for charged pions production $(\pi^+ + \pi^-)/2$ in proton-tungsten (pW) collision at $E_{LAB} = 400$ GeV at mid-rapidity. Data are from [55]. **Bottom**: The ratios data-to-theory as a function of transverse momentum p_T.

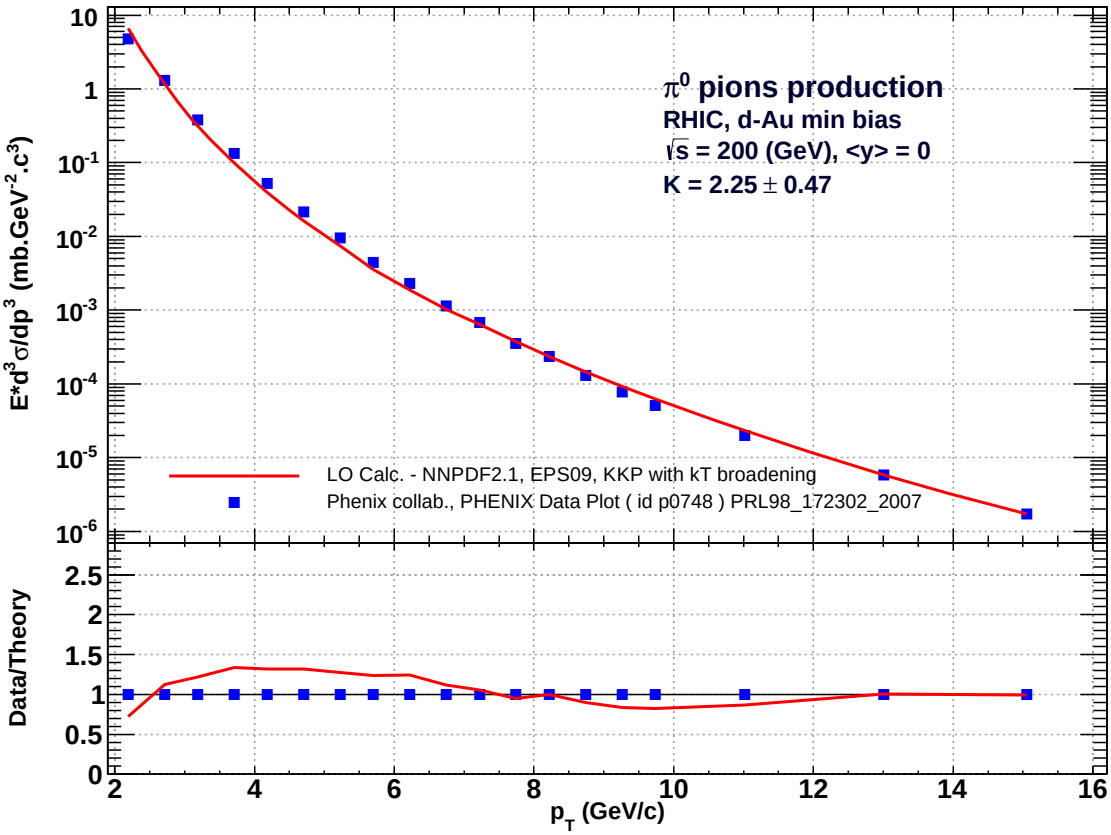

Figure 3.4: **Top**: Inclusive cross section for π^0 production in deuteron-gold (dAu) collision at $\sqrt{s} = 200$ GeV at mid-rapidity. Data are from experiment PHENIX [56]. **Bottom**: The ratios data-to-theory as a function of transverse momentum p_T.

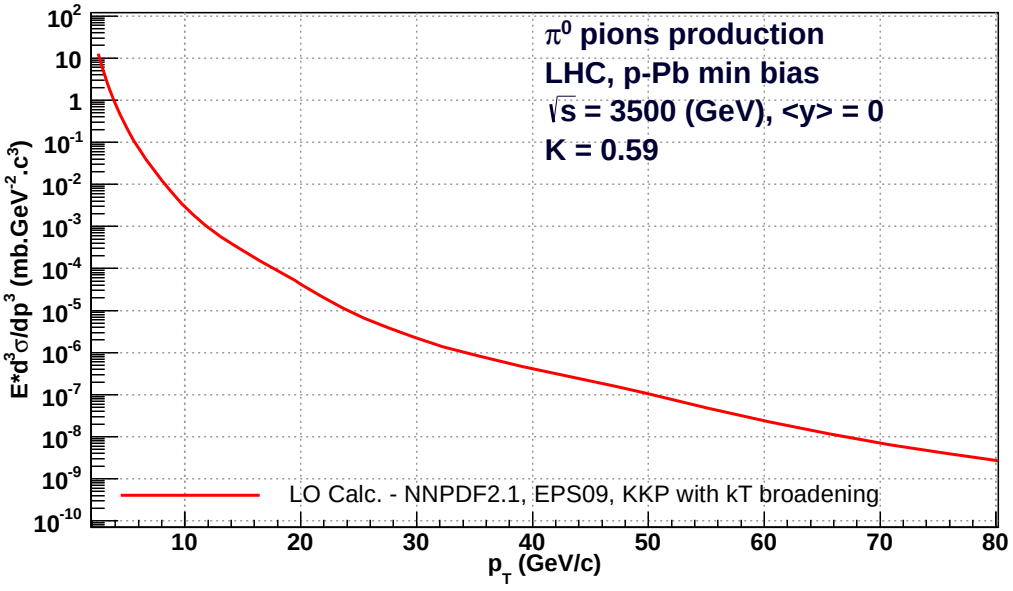

Figure 3.5: The prediction for inclusive cross section for π^0 production in proton-lead ($dpPb$) collision at $\sqrt{s} = 3500$ GeV at mid-rapidity for LHC. The K-factor 0.59 follows from the analysis in Sec. 2.8.

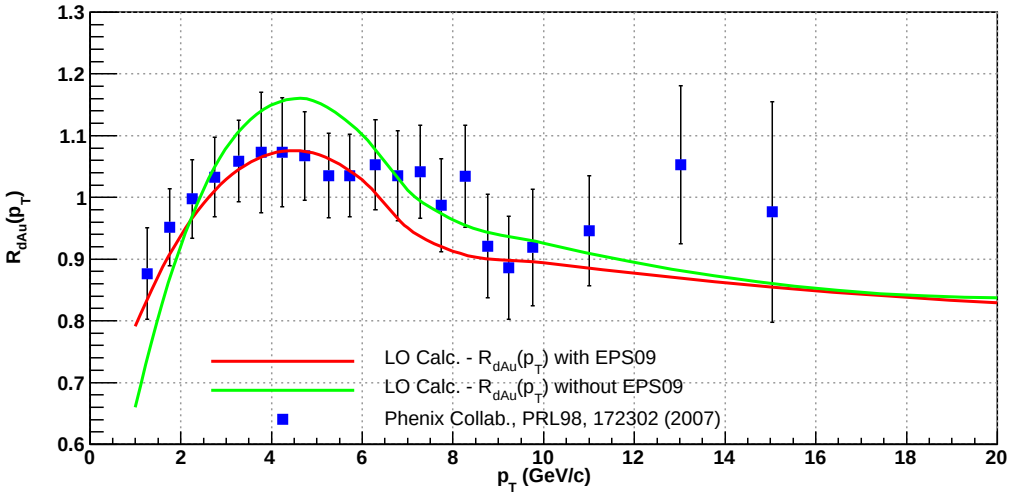

Figure 3.6: Nuclear modification factor R_{dAu} for π^0 versus p_T in deuteron-gold (dAu) collisions at RHIC at $\sqrt{s} = 200$ GeV at mid-rapidity. Data are from experiment PHENIX [56] with systematics errors.

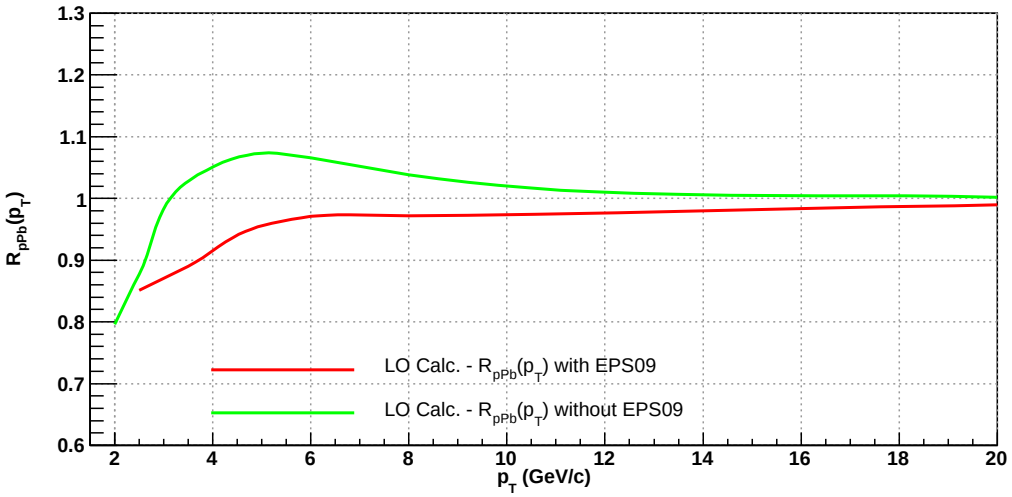

Figure 3.7: Prediction for nuclear modification factor R_{pPb} for π^0 versus p_T in proton-lead (pPb) collisions at LHC at $\sqrt{s} = 3500$ GeV at mid-rapidity.

Chapter 4

Conclusion

In the present diploma thesis the inclusive high-p_T particle production cross section in pp an pA collisions was studied. pp collisions were studied in the energy range corresponding to c.m. energy from $\sqrt{s} = 31.56$ to 7 TeV. Calculations were performed in the framework of the collinear QCD improved quark-parton model and the model including the intrinsic parton transverse momenta (k_T smearing). We used recent parton distribution functions NNPDF2.1 [22] and fragmentation functions KKP [24]. The partonic cross sections were calculated in the leading-order of the perturbative QCD.

For pp collisions we compared model calculations for p_T-dependent invariant cross section with E706, PHENIX, STAR, ALICE and CMS data and found a nice agreement. In comparison with collinear parton model the model with k_T smearing is proved to be more accurate for smaller transverse momenta.

The difference between computed and measured spectra is quantified in terms of the K-factor, $K = d\sigma^{exp}/d\sigma^{calc}$. The K-factor was investigated as a function of $\sqrt{s}$ and found to decrease with $\sqrt{s}$. We found also that the K-factor for collinear parton model is larger than for the model with k_T smearing, in accordance with [7].

In the second part of this diploma thesis we studied hadron production at large p_T in pA collisions. Here we used two nuclear effects in the parton model with k_T smearing: i) the parton nuclear broadening due to initial state multiple parton rescattering;ii) the nuclear parton distribution functions EPS09 [50]. We calculated the cross section for hight-p_T hadron production at $\sqrt{s}$ from 24 GeV to 3500 GeV in a good agreement with available data from Fermilab and PHENIX Collaboration. We evaluated also the nuclear modification factor R_{dAu} in a good agreement with RHIC data. Finally we performed for the first time predictions for this factor corresponding to pPb collisions in the LHC energy range. These results can be tested in the future by expected data from LHC experiments.

Bibliography

[1] D. J. Gross and F. Wilczek, Phys. Rev. Lett. **30**, 1343 (1973).

[2] H. D. Politzer, Phys. Rev. Lett. **30**, 1346 (1973).

[3] R. P. Feynman, *Photon-Hadron Interactions* (Reading, Mass.: W.A. Benjamin, 1972).

[4] J. D. Bjorken and E. A. Paschos, Phys. Rev. **185**, 1975 (1969).

[5] R. P. Feynman, R. D. Field, and G. C. Fox, Phys. Rev. D **18**, 3320 (1978).

[6] E. Reya, Phys. Rep. **69**, 195 (1981).

[7] J. F. Owens, Rev. Mod. Phys. **59**, 465 (1987).

[8] J. Collins, *Foundations of Perturbative QCD* (Cambridge University Press, New York, 2011).

[9] J. C. Collins, D. E. Soper, and G. F. Sterman, Adv.Ser.Direct.High Energy Phys. **5**, 1 (1988).

[10] P. Hanson, The Parton Model , (http://www-zeus.desy.de/∼liuc/physics/parton.pdf, 2004).

[11] B. R. W. R. K. Ellis, W. J. Stirling, *QCD and Collider Physics* (Cambridge University Press, 2003).

[12] J. Chýla, *Quarks, partons and Quantum Chromodynamics* (http://www-hep.fzu.cz/∼chyla/lectures/text.pdf, 2009).

[13] A. Lipatov, M. Malyshev, and N. Zotov, JHEP **1112**, 117 (2011), arXiv:1110.6582.

[14] G. Barnafoldi, P. Levai, G. Papp, G. I. Fai, and Y. Zhang, Heavy Ion Phys. **18**, 79 (2003), arXiv:nucl-th/0206006.

[15] X.-N. Wang, Phys. Rev. C **61**, 064910 (2000).

[16] J. F. Owens, E. Reya, and M. Glück, Phys. Rev. D **18**, 1501 (1978).

[17] V. N. Gribov and L. N. Lipatov, Sov. J. Nucl. Phys. **15**, 438 (1972).

[18] G. Altarelli and G. Parisi, Nucl. Phys. B **126**, 298 (1977).

[19] Y. L. Dokshitzer, Sov. Phys. JETP **46**, 641 (1977).

[20] J. Pumplin *et al.*, JHEP **07**, 012 (2002), arXiv:hep-ph/0201195.

[21] A. Martin, W. Stirling, R. Thorne, and G. Watt, Eur. Phys. J. C **63**, 189 (2009), arXiv:0901.0002.

[22] The NNPDF Collaboration, R. D. Ball *et al.*, Nucl. Phys. B **855**, 153 (2012), arXiv:1107.2652.

[23] R. Field and R. Feynman, Nucl. Phys. B **136**, 1 (1978).

[24] B. A. Kniehl, G. Kramer, and B. Potter, Nucl. Phys. B **582**, 514 (2000), arXiv:hep-ph/0010289.

[25] D. de Florian, R. Sassot, and M. Stratmann, Phys. Rev. D **75**, 114010 (2007), arXiv:hep-ph/0703242.

[26] F. M. Borzumati and G. Kramer, Z. Phys. C **67**, 137 (1995).

[27] X.-N. Wang, Phys. Rep. **280**, 287 (1997).

[28] X.-N. Wang, Phys. Rev. Lett. **81**, 2655 (1998).

[29] X.-N. Wang, Phys. Rev. C **58**, 2321 (1998).

[30] A. P. Contogouris, R. Gaskell, and S. Papadopoulos, Phys. Rev. D **17**, 2314 (1978).

[31] D. Sivers, S. J. Brodsky, and R. Blankenbecler, Phys. Rep. **23**, 1 (1976).

[32] J. F. Owens and J. D. Kimel, Phys. Rev. D **18**, 3313 (1978).

[33] L. Apanasevich *et al.*, Phys. Rev. D **59**, 074007 (1999).

[34] F. Diakonos, G. Galanopoulos, and X. Maintas, (2005), arXiv:hep-ph/0506010.

[35] X.-N. Wang and M. Gyulassy, Phys. Rev. D **44**, 3501 (1991).

[36] T. Sjöstrand and M. van Zijl, Phys. Rev. D **36**, 2019 (1987).

[37] A. C. Genz, Adaptive multidimensional integration subroutine, 1984, http://orion.math.iastate.edu/docs/cmlib/adapt/adapt.

[38] R. Piessens, E. de Doncker-Kapenga, and C. W. Ueberhuber, *Quadpack. A subroutine package for automatic integration* (Springer, 1983).

[39] Fermilab E706 Collaboration, L. Apanasevich *et al.*, Phys. Rev. D **68**, 052001 (2003), arXiv:hep-ex/0204031.

[40] PHENIX Collaboration, Pi0 cross section in pp collisions at sqrt(s)=62 gev at midrapidity, PHENIX Data Plot (id p0697).

[41] STAR Collaboration, B. I. Abelev *et al.*, Phys. Rev. C **81**, 064904 (2010).

[42] PHENIX Collaboration, S. S. Adler *et al.*, Phys. Rev. Lett. **91**, 241803 (2003).

[43] ALICE collaboration, Y. Kharlov, (2011), arXiv:1102.1840.

[44] CMS Collaboration, S. Chatrchyan *et al.*, JHEP **1108**, 086 (2011), arXiv:1104.3547.

[45] K. Eskola and H. Honkanen, Nucl. Phys. A **713**, 167 (2003).

[46] C. Salgado *et al.*, J. Phys. G **39**, 015010 (2012), arXiv:1105.3919.

[47] J. W. Cronin *et al.*, Phys. Rev. D **11**, 3105 (1975).

[48] H. D. Vries, C. D. Jager, and C. D. Vries, Atomic Data and Nuclear Data Tables **36**, 495 (1987).

[49] M. Arneodo, Phys. Rep. **240**, 301 (1994).

[50] K. Eskola, H. Paukkunen, and C. Salgado, JHEP **0904**, 065 (2009), arXiv:0902.4154.

[51] M. Hirai, S. Kumano, and T.-H. Nagai, Phys. Rev. C **76**, 065207 (2007), arXiv:0709.3038.

[52] K. Eskola, V. Kolhinen, and C. Salgado, Eur. Phys. J. C **9**, 61 (1999), arXiv:hep-ph/9807297.

[53] M. Johnson, B. Kopeliovich, and A. Tarasov, Phys. Rev. C **63**, 035203 (2001), arXiv:hep-ph/0006326.

[54] K. Golec-Biernat and M. Wüsthoff, Phys. Rev. D **59**, 014017 (1998).

[55] D. Antreasyan *et al.*, Phys. Rev. D **19**, 764 (1979).

[56] Phenix Collaboration, Kopeliovich *et al.*, PRL98 172302 (2007) .